DESIGN AND IMPLEMENTATION OF MICROSTRIP PATCH ANTENNAS FROM NARROWBAND TO ULTRA-WIDEBAND WITH HIGH INTERPORT ISOLATION FOR IN BAND FULL DUPLEX COMMUNICATION SYSTEMS

by

LÜTFİ YİĞİT EROL

Submitted to Graduate School of Engineering and Natural Sciences
in partial fulfillment of the requirements for the degree of
Master of Science

Sabancı University

August 2020

DESIGN AND IMPLEMENTATION OF MICROSTRIP PATCH ANTENNAS FROM NARROWBAND TO ULTRA-WIDEBAND WITH HIGH INTERPORT ISOLATION FOR IN BAND FULL DUPLEX COMMUNICATION SYSTEMS

APPROVED BY:

Prof. Dr. İbrahim Tekin.....
(Thesis Supervisor)

Assoc. Prof. Dr. Hüsnü Yenigün.....

Assoc. Prof. Dr. Nurhan Türker Tokan.....

DATE OF APPROVAL: 17.08.2020

ABSTRACT

DESIGN AND IMPLEMENTATION OF MICROSTRIP PATCH ANTENNAS FROM NARROWBAND TO ULTRA-WIDEBAND WITH HIGH INTERPORT ISOLATION FOR IN BAND FULL DUPLEX COMMUNICATION SYSTEMS

LÜTFİ YİĞİT EROL

M.Sc. Thesis, August 2020
Supervisor: Prof. Dr. İbrahim Tekin

Keywords: In band full duplex communication, self-interference cancellation, microstrip patch antenna, differentiation circuit, high isolation, ultra-wideband, balun

One of the most useful solutions for enhancing the throughput and spectral efficiency wireless communication networks is in band full duplex (IBFD) operation. Receiving and transmitting radio frequency (RF) signals simultaneously in the same frequency band is one of the best advantages of IBFD. However, there are many challenges for the implementation of IBFD operation; one of them is self-interference (SI).

In general, the improvement of the throughput and the spectral efficiency of a communication system is directly proportional to high signal to noise ratio (SNR). To achieve a great SNR value, SI should be suppressed to noise floor. In IBFD communication systems, most of the SI cancellation is provided at the antenna side. Thereby, the implementation of an antenna with very high isolation offers a great solution for IBFD communication systems.

In this thesis, the microstrip patch antennas from narrowband to ultra-wideband are designed and implemented to use in IBFD operation. The implemented 2.4 GHz and 5.8 GHz IBFD differential fed microstrip patch antenna arrays and 2.4 GHz IBFD double differential fed microstrip patch antenna achieve interport isolation of 53, 51 and 62 dB over their operating bandwidths of 50, 200 and 50 MHz, respectively. On the other hand, the implemented ultra-wideband (UWB) IBFD antenna provides interport isolation of 30 dB for its 4.9 GHz of 10 dB return loss bandwidth (2.3 – 7.2 GHz). This antenna may be used for all of the Wi-Fi bands including the next generation IEEE 802.11be whose possible need will be full-duplexity.

ÖZET

BAND İÇİ TAM ÇİFT YÖNLÜ HABERLEŞME SİSTEMLERİ İÇİN PORTLAR ARASI İZOLASYONU YÜKSEK DAR BANTTAN ÇOK GENİŞ BANTA KADAR MİKROŞERİT YAMA ANTENLERİN TASARIMI VE GERÇEKLENMESİ

LÜTFİ YİĞİT EROL

Yüksek Lisans Tezi, Ağustos 2020
Tez Danışmanı: Prof. Dr. İbrahim Tekin

Anahtar Kelimeler: Band içi tam çift yönlü haberleşme, öz girişim iptali, mikroşerit yama anten, fark devresi, yüksek izolasyon, çok geniş bantlı, balun

Band içi tam çift yönlü (IBFD) operasyonu kablosuz haberleşme sistemleri ve ağlarının spektral verimliliğini ve toplam sistem kapasitesini arttıran cazip çözümlerden bir tanesidir. IBFD operasyonun en iyi avantajlarından bir tanesi ise radio frekans (RF) sinyallerinin aynı frekans bandında eş zamanlı olarak alımı ve gönderimidir. Ancak, IBFD operasyonunun gerçekleştirilmesinin birçok zorluğu vardır, bunlardan biri ise öz girişimdir.

Genel olarak, bir haberleşme sisteminin spektral verimliliğinin ve toplam sistem kapasitesinin gelişmesi yüksek bir sinyal gürültü oranı ile doğru orantılıdır. Yüksek bir sinyal gürültü oranını tutturmak için öz girişimin gürültü seviyesine kadar bastırılması gerekir. IBFD haberleşme sistemlerinde öz girişim iptalinin büyük bir bölümü anten kısmında sağlanmaktadır. Bu sebeple, çok yüksek izolasyona sahip bir antenin gerçekleştirilmesi IBFD haberleşme sistemleri için mükemmel bir çözüm sunar.

Bu tezde, IBFD operasyonunda kullanılmak üzere dar banttan çok geniş banta kadar çalışan mikroşerit yama antenler tasarlanmış ve gerçeklenmiştir. Gerçeklenen 2.4 GHz ve 5.8 GHz IBFD diferansiyel beslemeli mikroşerit yama anten dizileri ve 2.4 GHz IBFD çift diferansiyel beslemeli mikroşerit yama anten 50, 200, ve 50 MHz çalışma bant genişliğinde sırasıyla 53, 51 ve 62 dB portlar arası izolasyon değerlerini başarmaktadırlar. Diğer yandan, gerçeklenen çok geniş bantlı IBFD anten 4.9 GHz'lik çalışma bant genişliğinde (2.3 – 7.2 GHz) 30 dB portlar arası izolasyonu sağlamaktadır. Bu anten bant içi tam çift yönlü yapıya ihtiyaç duyacak olan gelecek nesil IEEE 802.11be standardı da dahil olmak üzere tüm Wi-Fi bantlarında kullanılabilir.

ACKNOWLEDGEMENTS

Firstly, I would like to express my gratitudes to my thesis supervisor Prof. Dr. Ibrahim Tekin for his guidance about the subject of this thesis. I have enjoyed at every stage of this research, so I would like to thank him since he had given me this chance. I also appreciate my jury members Assoc. Prof. Dr. Hüsnü Yenigün and Assoc. Prof. Dr. Nurhan Türker Tokan (Yıldız Technical University) for their attendance.

I would like to acknowledge Dr. Haq Nawaz since he had encouraged me in the first year of my master's education and also inspired for designs of some of the antennas proposed in this thesis. I also thank Abdulkadir Uzun for his help during the measurements of fabricated antennas. I appreciate Asst. Prof. Dr. Halit Cenan Mertol for his support during the general overview of the thesis.

I would like to give props to Ercan Güldoğan and Prof. Dr. Gökhan Göktuğ for playing a very big role for my master’s degree education.

I would like to thank my brothers Oğulcan, Alp, Emir, Mert, Meriç, and Onurcan. They have always supported and encouraged me in my life. They are my family and I feel so lucky for being their friend. Also, I would like to thank Hazal for believing me at every stage of this thesis and my life.

My family has always supported me in every stage of my life. Therefore, I would like to thank my father Dr. Ahmet Hakan Erol. I also greet all my family members with respect.

And most of all, I would like to thank my mother Sema Esin Sağlam. She had grown, taught, and loved me. Without her, I cannot achieve anything in my life. Honestly, I owe her everything, that’s why I would like to express my biggest gratitudes and appreciations to my mother.

TABLE OF CONTENTS

Page

LIST OF FIGURES

Page

LIST OF TABLES

Page

ABBREVIATIONS

Abbreviation	Description
IBFD	In Band Full Duplex
SI	Self-Interference
RF	Radio Frequency
dB	Decibel
UWB	Ultra-wideband
MHz	Mega Hertz
GHz	Giga Hertz
Tx	Transmitter
Rx	Receiver
PCB	Printed Circuit Board
CW	Continuous Wave
WLAN	Wireless Local Area Network
LC	Inductor – Capacitor
SNR	Signal to Noise Ratio
FDD	Frequency Division Duplexing
balun	Balanced to Unbalanced Transformer
Freq	Frequency
sim	Simulated
mea	Measured
ε_r	Dielectric Constant

1. INTRODUCTION

There are three types of telecommunication systems based on the way of connection: simplex, half-duplex and full-duplex. The type of simplex is the communication in one direction only. Television systems and radio broadcasts fall into this category. Half-duplex operation is the communication in both directions, but not simultaneously. The device of walkie-talkie falls into this category. In full-duplex operation, communication realizes in both directions, simultaneously. A mobile phone is the best example given for full-duplex communication systems.

In band full-duplex (IBFD) communication is one of the desirable solutions for enhancing the efficiency and the throughput of wireless communication systems and networks. One of the advantages of IBFD communication is to transmit and receive simultaneously on the same frequency band, which is a great offer for wireless networks. However, there are lots of challenges for the implementation of IBFD communication such as self-interference (SI). IBFD has, until recent times, not used greatly because of the potential weaken effects of SI. Therefore, IBFD communication can be successful by minimizing SI. There are many ways to implement SI cancellation. Some of these ways are wireless-propagation-domain techniques, analog-circuit-domain techniques, and digital-domain techniques [1].

Recently, there have been many researches to improve IBFD communication systems. Wi-Fi is a type of half-duplex communication, while Ethernet falls into full-duplex operation. In Figure 1.1, the working principles of these two networks are shown. In Wi-Fi, transmitting and receiving realize at different times, while they realize simultaneously in Ethernet. As known, Ethernet provides a more efficient connection than Wi-Fi, due to its better spectral efficiency and throughput. However, there is a remarkable interest in

re-designing half-duplex communication systems, such as Wi-Fi and cellular systems. This can be realized leveraging IBFD [1]. The main idea is IBFD communication systems will have a critical role for the next generation (5G) mobile networks.

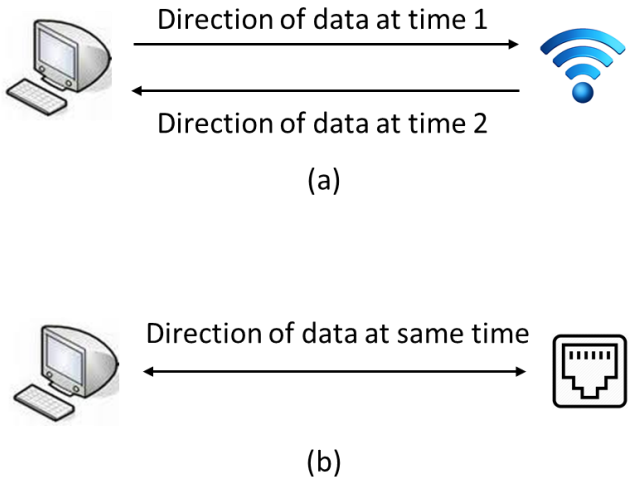

Figure 1.1: Data transmission in (a) Wi-Fi and (b) Ethernet

Wi-Fi is a member of wireless network protocols and is one of the most common ways that are used for local area networking (LAN) of devices. It has become a very preferred technology in both business and home environments, and it is one of the spectacular areas in the communication systems [2,3]. Wi-Fi uses many parts of IEEE 802.11 standard including 802.11n (Wi-Fi 4), 802.11ac (Wi-Fi 5), and 802.11ax (Wi-Fi 6). 802.11be which is also called Wi-Fi 7 is considered as the next member of Wi-Fi standardization [4]. Table 1.1 shows all official Wi-Fi generations, corresponding IEEE standards, and their frequency bands.

Table 1.1: Wi-Fi generations and their frequency bands

Generation	IEEE Standard	Frequency Band
Wi-Fi 4	802.11n	2.4/5 GHz
Wi-Fi 5	802.11ac	5 GHz
Wi-Fi 6	802.11ax	2.4, 5, 6 GHz
Wi-Fi 7 [4]	802.11be	2.4, 5, 6, 7 GHz

1.1.Motivation of Thesis

In this thesis, IBFD communication systems and SI, which is the main challenge for IBFD communication systems will be introduced. Our purpose is to design and fabricate microstrip patch antennas that operate at 2.4 and 5.8 GHz, which are WLAN frequencies according to the IEEE 802.11 standard. As discussed earlier, 4G mobile networks work with half duplex operation, our idea is to improve IBFD operation for 4G mobile networks. Another purpose is to implement an antenna which can be used for all of the Wi-Fi bands of IEEE 802.11 standard, including 3.6 GHz and sub-6 GHz band of 5G applications.

Due to increase interport isolation of microstrip patch antennas, we benefit from differential feeding networks. Fabricated antennas for 2.4 and 5.8 GHz applications provide high interport isolation which offers a good solution for IBFD communication systems. On the other hand, the implemented ultra-wideband (UWB) IBFD antenna can be a great candidate for next generation IEEE 802.11be which is also called as Wi-Fi 7.

1.2. Organization of Thesis

The first chapter briefly summarizes telecommunication systems based on the way of connection. The advantages of IBFD communication systems and self-interference which is the main challenge of this system are introduced. In this chapter, we mention our motivation for designing and fabricating microstrip patch antennas. The organization of the thesis is also introduced in this chapter.

The second chapter mentions the main challenge of IBFD communication systems – Self-Interference. In this chapter, SI cancellation techniques as separate antenna structure and single/shared antenna structure will be introduced. After, we will mention some researches that refer to SI cancellation techniques. Finally, we will summarize the usage areas of antennas in IBFD communication systems.

In third chapter, the design and simulation details of the reported narrowband microstrip patch antennas are presented. There are three proposed narrowband microstrip patch antennas in this thesis – 2.4 GHz IBFD Differential Fed Microstrip Patch Antenna Array, 5.8 GHz IBFD Differential Fed Microstrip Patch Antenna Array, and 2.4 GHz IBFD Double Differential Fed Microstrip Patch Antenna. Simulation results for S-parameters, radiation patterns, co-polarization, and cross-polarization gain patterns of reported narrowband antennas are introduced in this chapter.

In fourth chapter, antenna port matching and interport isolation measurement results of microstrip patch antennas presented in third chapter are discussed. Dimensions and fabrication details of proposed antennas are introduced in this chapter. All of the antennas were measured at the laboratory environment, measurement results are also compared with simulation results.

In fifth chapter, the design details, simulations, and measurements of the UWB IBFD antenna are introduced. The proposed UWB IBFD antenna provides much more 10 dB return loss bandwidth compared to other reported antennas. It consists of three port radiating element with a UWB balun to create the differential feeding network. Since its design and structure are little different from other introduced antennas, the UWB IBFD antenna is presented in a different chapter.

In sixth chapter, the thesis will be concluded. The measurement results of fabricated microstrip patch antennas will be briefly summarized and we will mention the future work for improving these designs.

2. SELF-INTERFERENCE CHALLENGE FOR IBFD COMMUNICATION SYSTEMS

IBFD communication provides many advantages; it increases spectral efficiency and throughput. In IBFD communication, receiver and transmitter operate at the same frequency with the same bandwidth. The main limitation of IBFD communication is SI. SI must be minimized for IBFD communication to reach its maximum efficiency. For example, in Wi-Fi, the transmit power can reach to 20 dBm for 10 MHz bandwidth [5]. The typical noise floor is approximately -90 dBm, that means more than 110 dB for 10 MHz bandwidth of SI cancellation is necessary for appropriate operation of IBFD as shown in Figure 2.1. In case the SI cancellation does not reach this value, the signal to noise ratio (SNR) decreases, so, it impacts negatively the throughput of communication. Therefore, to minimize SI is one of the most important challenges for IBFD communication.

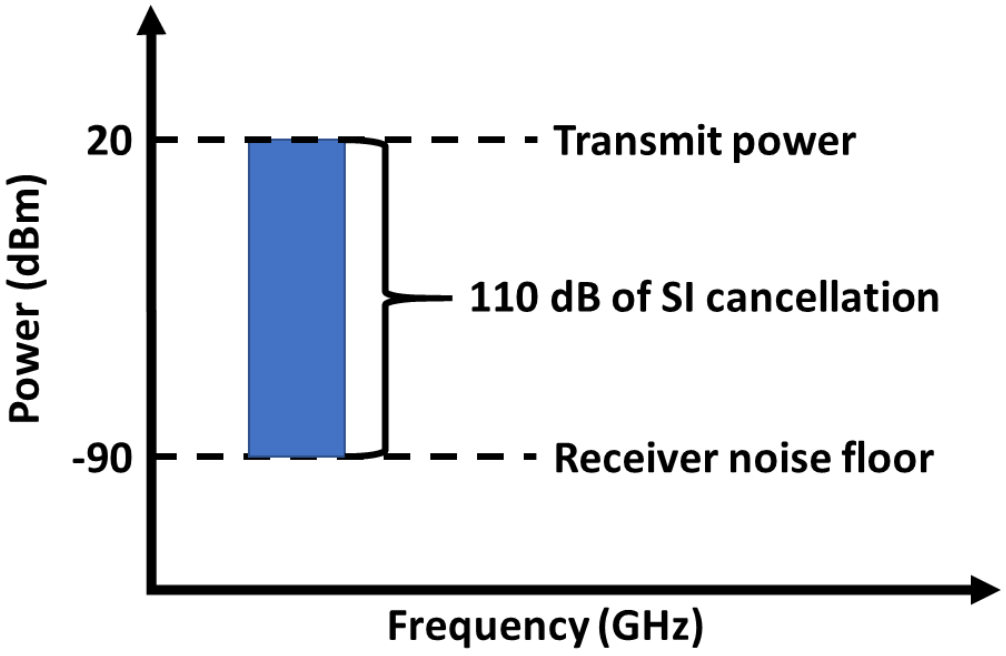

Figure 2.1: Required SI cancellation for Wi-Fi

2.1. Self-Interference Cancellation Techniques

One can design an antenna with its transmitter and receiver parts in two different forms: the separate antenna structure and the single/shared antenna structure [6].

2.1.1. Separate Antenna Structure

More than one antenna which are receive and transmit antennas are used for the separate antenna structure. Generally, isolation between these antennas is supplied by increasing the path loss between them. SI may be cancelled with three SI cancellation techniques listed below [6]:

- Arranging the distance between transmitter and receiver antennas
- Locating the transmitter and receiver on the opposite side of the wireless device
- Benefiting from directional antennas

These three passive SI cancellation techniques are shown in Figure 2.2.

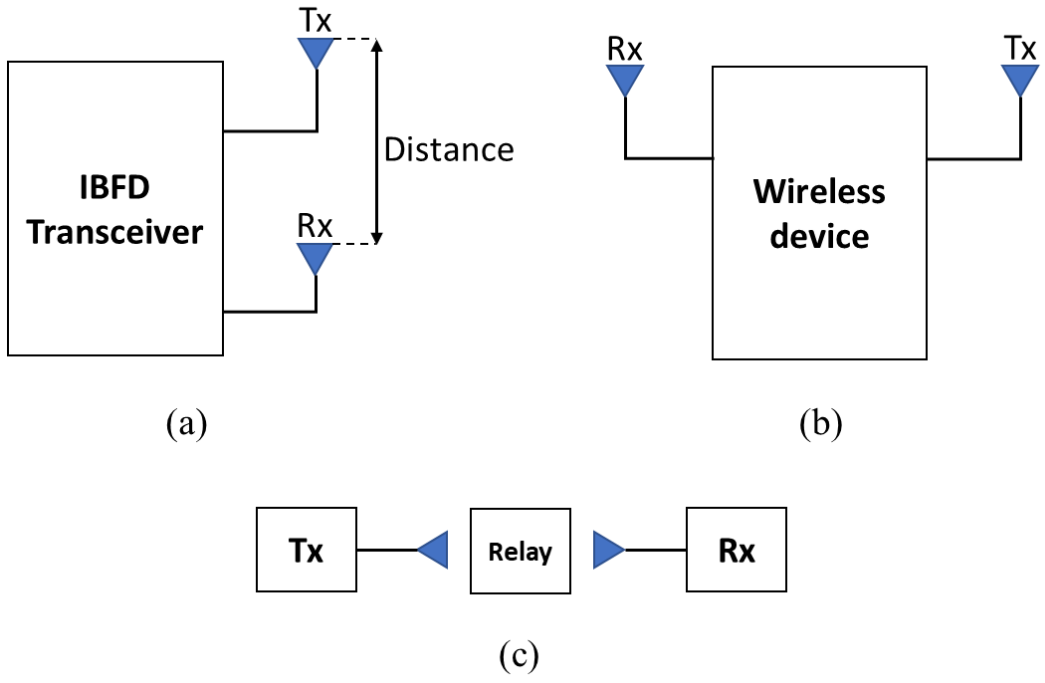

Figure 2.2: Passive SI cancellation techniques (a) arranging the distance (b) locating Tx and Rx at opposite sides (c) benefiting from directional antennas

Benefiting from directional antennas technique is generally seen in Full Duplex Relaying (FDR). FDR dramatically minimizes SI, so it improves the spectral efficiency and throughput of wireless networks [7].

2.1.2. Single/Shared Antenna Structure

Transmitter and receiver locate at common antenna in the shared antenna structure. Figure 2.3 shows a block diagram of a conventional half duplex system implemented with Frequency Division Duplexing (FDD) [8]. As can be seen, the system has a frequency duplexer which dispatches the signals of power amplifier at transmitter (Tx) side to low noise amplifier at receiver (Rx) side. This filter is formed to ensure acceptable isolation between Tx and Rx by decreasing the RF leakage. Since Tx and Rx operate at different frequencies, high isolation between these two parts can be clearly achieved by the duplexer.

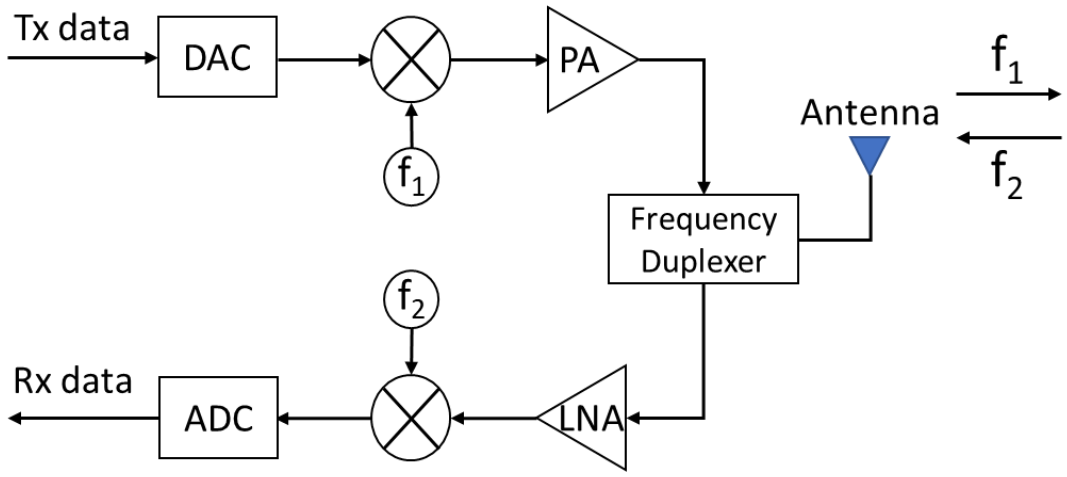

Figure 2.3: Block diagram of half duplex transceiver by using FDD

Figure 2.4 shows a block diagram of a full duplex system whose Tx and Rx operate at the same frequency band. As shown, a three-port routing device is used instead of the frequency duplexer. The routing device is generally called as circulator, moreover, it can also be a directional coupler or a hybrid coupler, which can route the signals from power amplifier at Tx side to low noise amplifier at Rx side, simultaneously.

Here, the mission of three port routing device should be to obtain high isolation between Tx and Rx. One can implement an IBFD transceiver whose transmitter and receiver operate at the same frequency, by using this structure.

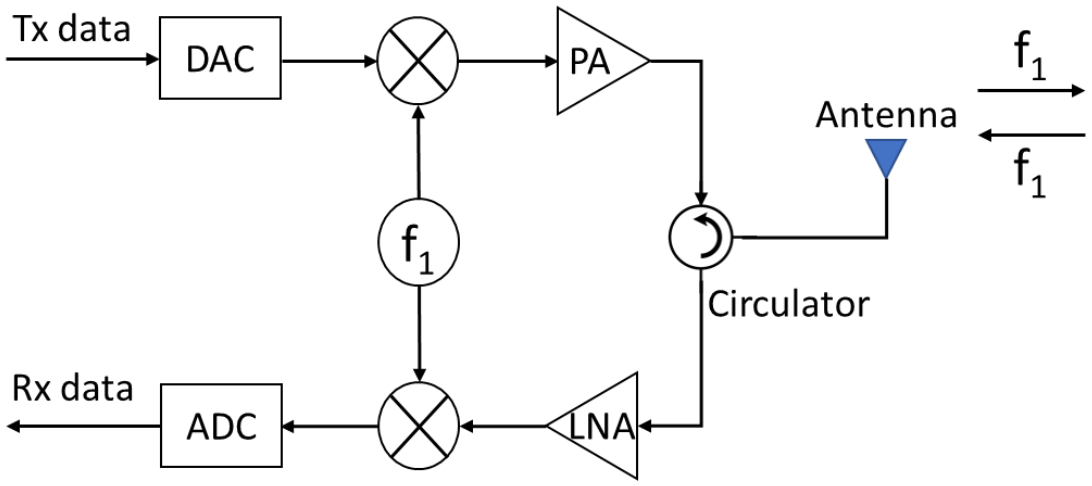

Figure 2.4: Block diagram of full duplex transceiver by using three-port routing device

2.2. Literature Review of Self-Interference Circuits

A raft of SI cancellation techniques for IBFD system has been proposed recently. In general, SI cancellation techniques are divided into two different categories: passive suppression techniques and active cancellation techniques. Typical IBFD communication systems can perform both these techniques to achieve remarkable SI cancellation.

The SI is cancelled in the propagation domain before it is received by Rx for passive suppression techniques [9]. It can be achieved by using antenna separation or using more than one antenna with correct position or using directional antennas, as discussed before. Slingsby et al. [10] reach to isolation of 85 dB between directional receive and transmit antennas which are separated by 5 meters with shielding between them. They also observe that the isolation would dramatically decrease if these antennas were closer. Anderson et al. [11] also achieve 85 dB of interport isolation with vertical antenna separation of 3.5 – 6 meters. Haneda et al. [12] provide isolation of 70 dB between Tx and Rx antennas with separation of 5 meters.

Separate antenna structure has a significant role on SI cancellation, however, the passive cancellation achieved by using antenna separation is very limited in mobile applications since these applications are implemented using small device dimensions. Moreover, the value of isolation does not depend on only separation of antennas, it depends on many factors. Everett et al. [13] investigate the factors that affect antenna isolation. In their experiments, they benefit from L-com HG2414DP-090 panel antennas [14] implemented for outdoor applications of Wi-Fi. In experiments performed inside anechoic chamber (AC), they compare isolation values of three situations. First of all, they provide 45 dB of isolation with 50 cm of antenna separation without any absorber (A). When they use an absorber as a shield, they see that isolation has increased to 55 dB. After they re-design panel antennas as dual-polarized due to implement cross-polarization (CP). Without any shielding, dual-polarized antennas with 50 cm separation provide 64 dB of isolation. Dual polarized antennas with shielding between them ensure 74 dB of isolation. In short, they increase antenna isolation from 46 dB to 74 dB by courtesy of implementation of absorber and cross-polarization. Furthermore, they research effects of environmental reflections. When they perform measurements in reflective room (RR), dual polarized antennas with absorbers provide only 46 dB, this value was 74 dB inside anechoic chamber, as discussed earlier. Provided antenna isolations by Everett et al. [13] are shown in Table 2.1.

Table 2.1: Provided isolation values by Everett et al. [13]

	Inside AC	**In RR**
Initial state	45 dB	38 dB
With A	55 dB	40 dB
With CP	64 dB	45 dB
With CP and A	74 dB	46 dB

The other antenna cancellation technique is discussed in [15]. This technique operates cancellation with three antennas to create radiation pattern void which cancels the SI at the receive antenna. It also uses antenna separation as cancellation technique. Figure 2.5 shows that two of the three antennas are transmitters located at a distance “d” and

"d + λ/2" apart from Rx antenna, for a wavelength of λ. Tx antennas are located to cancel out each other, they cause a null position for receiver to receive much weaker signals. This antenna cancellation achieves 20 dB reduction in SI. The design can cancel 50-60 dB of SI with the combination of analog and digital cancellation circuits.

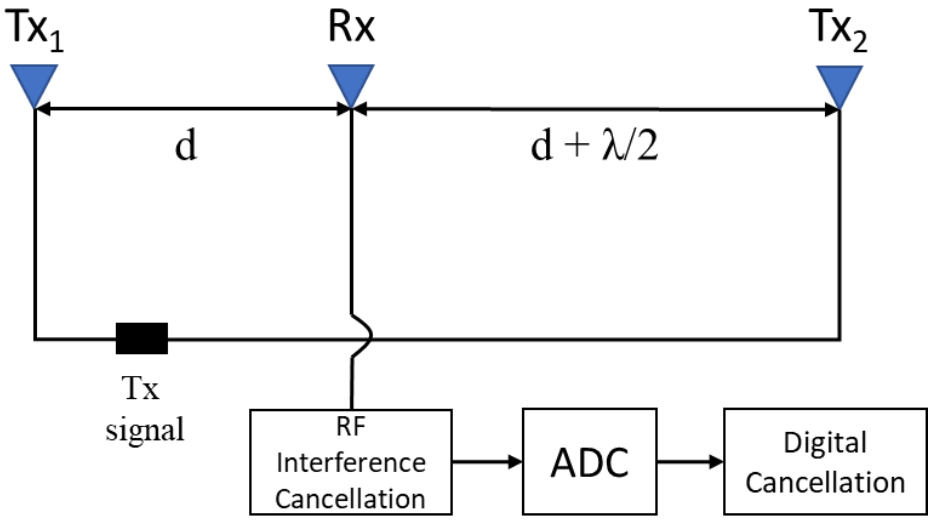

Figure 2.5: Block diagram of Multiple antenna SI cancellation

Jain et al. [15] also introduce to Balanced to Unbalanced Transformer (balun) cancellation. A balun has equal power outputs with 180^0 phase difference. They compare balun and phase offset based on SI cancellation. They show that balun can provide more SI cancellation for much wider bandwidth. Balun based cancellation provides the cancellation of 53 dB for 5 MHz bandwidth and 40 dB for 100 MHz bandwidth, while this value is only 24 dB for phase offset. They demonstrate that balun cancellation could work on wideband with high power signals.

Another research about balun based cancellation is introduced in [16]. Li et al. show that balun cancels at least 45 dB of SI and after arranging 20 centimeters of antenna separation, the residual SI is simulated as -71 dBm, where noise floor was approximately -90 dBm. Here, we can clearly say that balun based cancellation is very appropriate technique for mobile applications implemented using small device dimensions.

For shared-antenna-architecture, most of the reported antennas ensure high isolation between ports by polarization diversity. Nawaz et al. [17] introduce two microstrip patch antennas which achieve high isolation, both operate at 2.4 GHz. They benefit from balun based cancellation. The interport isolation is reached by combination of three port radiating elements and the hybrid ring coupler as a balun circuit. Two ports of radiating elements are differentially fed by connecting ring hybrid coupler between them. The input of ring hybrid coupler is receive port, while third port of radiating element is transmit port. They fabricate dual polarized microstrip patch antennas which provide 62 dB and 70 dB for 50 MHz bandwidth. One of their antennas which is designed as slot-coupled provides 90 dB of peak isolation. Their implemented antennas have a very low cross-polarization level.

Another shared antenna structure with high interport isolation is presented in [18]. This time, Nawaz et al. design four port radiating element. Double differential feeding is ensured by using two identical ring hybrid couplers as SI cancellation circuit, they are connected to parallel ports. Consequently, the double differential fed microstrip patch antenna provides the isolation of 72 dB over the antenna input bandwidth. The peak isolation is 98 dB, which is the best value of RF cancellation reported for a microstrip patch antenna with single/shared antenna structure. This work is the inspiration of this thesis.

In [6], dual port dual-polarized 2x1 antenna array is introduced, which is also the inspiration of the thesis. The ring hybrid coupler is again used as SI cancellation circuit in this work. Here, the antenna array has three ports with $\lambda/4$ feeds, two of these ports are connected to 180^0 hybrid coupler as an SI cancellation circuit. The input port of 180^0 hybrid coupler is used as Rx, while the third port of antenna array is used as transmit port. Implemented antenna array operates at 2.5 GHz and provides 60 dB of interport isolation for 50 MHz bandwidth. The antenna achieves high gain because of the array usage.

In the literature, most of the reported IBFD antennas operate over a narrow bandwidth. The reported IBFD antennas that operate over wider bandwidth provide less interport isolation than narrowband antennas. The proposed UWB simultaneous transmit and

receive (STAR) antenna in [19] provides higher than 40 dB between 0.6 and 1.75 GHz. The reported antenna consists of a monocone and a circular array. The reported antenna provides the peak realized gain of almost 5.5 dBi.

Deo et al. [20] implement the orthogonally polarized rectangular spiral antenna. They fed the antenna from the center of bottom layer with a coaxial cable. The measured peak gain of the antenna is 7 dBi, furthermore, the proposed antenna obtains better than 21.5 dB of isolation over its antenna 10 dB input bandwidth of 2.2 GHz (between 2.5 and 4.7 GHz). Also, it achieves 33.5 dB of isolation between ports for narrow bandwidth of 700 MHz (4 – 4.7 GHz).

The introduced wideband planar antenna in [21] includes radiating elements and differential feeding circuits. In the reported antenna, the radiating elements are symmetrically located onward the center of a circle. As a SI cancellation circuit, two identical 180^0 power dividers are used to feed the radiating elements. The introduced antenna operates between 6 and 7.2 GHz with the measured interport isolation of 40 dB. Moreover, it provides more than realized gain of 8.7 dBi including the losses of SMA cables and connectors.

Prasannakumar et al. [22] design and implement circularly-polarized reflector antennas with 10 dB impedance bandwidth of 4 GHz (4 – 8 GHz). It achieves more than 30 dB of interport isolation over its operating frequency range. In addition, the realized gain of 21 dBi is provided over its frequency range. The reported antenna benefits from 90^0 and 180^0 couplers and circulators in order to increase the interport isolation.

Another work presented in [23] consisted of a thin rectangular cavity with the slot lines is designed for IBFD communication systems. Although simulated S-parameter results show that 89 dB of interport isolation can be achieved; due to fabrication defects, more than 54 dB of isolation level over 8 dB impedance bandwidth (2.4 GHz) is obtained by the fabricated antenna.

2.3.Usage Areas of Implemented Antennas in IBFD Communication Systems

Implemented microstrip patch antennas in this thesis can be used for many IBFD operations due to their high interport isolation. In this section, some wireless communication networks for which the implemented microstrip patch antennas may be used are discussed. Some of these as IBFD wireless systems are full-duplex radars, full-duplex relaying systems, and cognitive radios. In addition to these systems, implemented antennas can be have a part in many other IBFD communication systems.

2.3.1. Full-Duplex Radar Systems

Basically, continuous-wave (CW) radar systems divide into two categories according to the number of antennas used: monostatic and bistatic. While monostatic CW radar systems use one single/shared antenna, bistatic CW radars use two different antennas which are Tx and Rx. The antenna used in monostatic CW radar systems acts both as transmitter and as receiver. In bistatic CW radar systems, an antenna behaves as Tx and the other antenna acts as Rx. Each of these antennas receives and transmit simultaneously [24]. Figure 2.6 shows two methods of interfacing antennas to full-duplex radar systems.

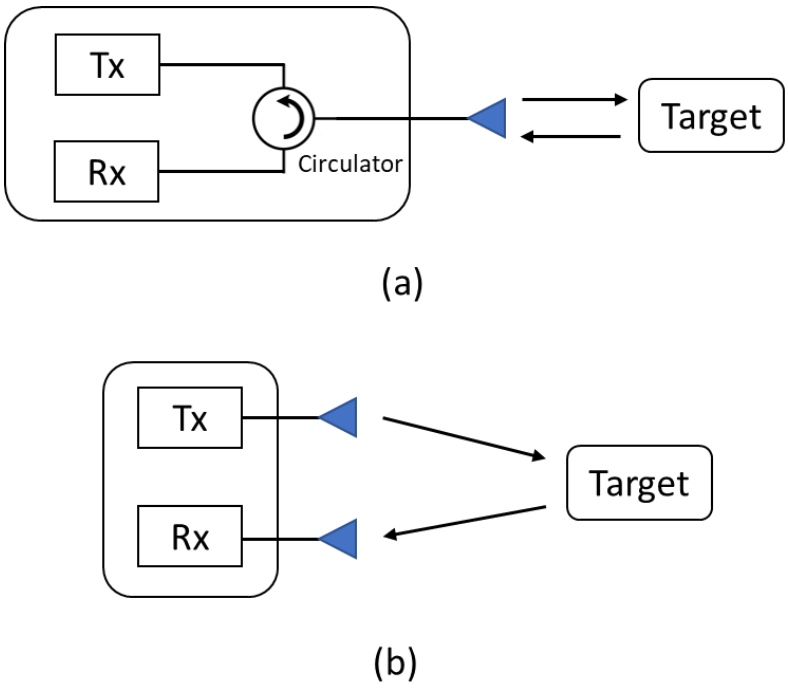

Figure 2.6: Two methods interfacing antennas to full-duplex radar systems (a) monostatic radar (b) bistatic radar

In the radar literature, SI is named as transmitter leakage [25]. The transmitter leakage is one of the main problems for implementation of CW radar systems. For bistatic CW radar systems, the isolation between Tx and Rx is achieved by adjusting the physical separation between them, while circulators are used in the case of monostatic radars [1]. These structures are also shown in Figure 2.6. Implemented antennas in this thesis which use shared antenna structure can be used for 2.4 GHz and 5.8 GHz monostatic CW radar applications.

2.3.2. Full-Duplex Relay (FDR) Systems

Relay technology is the one of the crucial applications for wireless communication systems. In relaying, in-band repeaters are benefited for enhancing the coverage area by receiving and transmitting simultaneously the amplified signal at the same frequency band [1]. The earliest and most known SI suppression technique for IBFD relays is to enhance physical separation between Tx and Rx antennas [26]. Moreover, several SI suppression techniques including digital and analog techniques have also been proposed [27,28]. SI reductions are also possible with the use of antenna arrays which permit beamforming-based SI negation [29]. A basic full-duplex relaying system can be implemented with microstrip patch antenna arrays proposed in this thesis, that operate at 2.4 and 5.8 GHz, moreover, the reported UWB IBFD antenna may be used for wideband FDR systems.

2.3.3. Cognitive Radios

Cognitive radio is an adaptive smart radio and network system which can determine available and unused channels in a wireless spectrum. This system enables more efficient communication by changing transmission parameters [30]. Cognitive radio systems lead to the best promising systems for future wireless communication networks. [31]. One of the main challenges in dynamic spectrum access is to detect when the secondary users can access to spectrum. In [32], some wireless communications schemes for cognitive radio are proposed by combining the several cancellation techniques for secondary users. The implemented antennas as IBFD transceivers can be used in cognitive radios.

2.3.4. The Next Member of WLAN: IEEE 802.11be

According to Wi-Fi Alliance [3], so many Wi-Fi devices including computers, smartphones, televisions, sensors, and other many systems are widely used throughout the world. The main focus of IEEE 802.11ax also called as Wi-Fi 6 is the user experience and the network performance, however, an extremely high throughput is necessary for the applications like ultra-quality videos, whose data rate reaches to 20 Gbps [33]. Moreover, low-latency operations such as augmented reality, virtual reality [34], and online conferences also require ultra-high throughput. Since Wi-Fi 6 cannot meet these requirements, IEEE 802.11 task group has determined [35] the creation of a new task group whose name is IEEE 802.11be also called as Wi-Fi 7.

According to the project authorization form [36], determining an ultra-high throughput as at least 30 Gbps at 1 – 7.25 GHz of frequency range is the main purpose of the IEEE 802.11be standard. Another focus is to make this standard backward-compatible with all IEEE 802.11 standards for all of licensed and unlicensed frequency bands.

There are lots of candidate technical features including simultaneously transmitting and receiving at different frequency bands for the next generation IEEE 802.11be standard discussed by several industrial and academic experts [37]. Transmitting and receiving at the same time in different frequency bands may decrease the latency and increase the system throughput by allowing simultaneous uplink/downlink operations at different bands [38]. As mentioned before, this process can be implemented with IBFD operation.

An antenna operating at a wide frequency range with high interport isolation can offer a great solution for the next generation IEEE 802.11 standard which is 802.11be. The UWB IBFD antenna reported in this thesis may be used for Wi-Fi 7 applications because it operates at 2.4, 5, 6, and 7 GHz of frequency bands providing high interport isolation and realized gain.

3. DESIGN DETAILS AND SIMULATION ANALYSIS OF MARCHAND COUPLER AND PROPOSED MICROSTRIP PATCH ANTENNAS

In this chapter, design details and simulation results of Marchand coupler and proposed microstrip patch antennas are introduced. Designed antennas provide high interport isolation using shared antenna structure with Marchand coupler as external SI cancellation circuits. All designed antennas provide low co-polarization. High Frequency Structure Simulator (HFSS) [39] is used for the design and simulation process of the proposed antennas. 1.6 mm thick FR4 material (ε_r=4.4, tangent loss=0.02) is used as a substrate. Totally, there are three designs which operate 2.4 GHz and 5.8 GHz of frequencies. This chapter consists of three sections:

(i) Design details and simulation analysis of Marchand coupler
(ii) Design details and simulation analysis of 2.4 GHz IBFD differential fed microstrip patch antenna array
(iii) Design details and simulation analysis of 5.8 GHz IBFD differential fed microstrip patch antenna array
(iv) Design details and simulation analysis of 2.4 GHz IBFD double differential fed microstrip patch antenna
(v) Design details and simulation analysis of 3.6 GHz double differential fed microstrip patch antenna

3.1. Marchand Coupler

A balun circuit can be used to perform differential feeding between ports of microstrip patch antennas since balun has equal power outputs with 180^0 of phase difference. There are lots of types of microstrip balun including hybrid coupler, coupled-line coupler, and microstrip based LC balun [40]. One of the advantages of Marchand coupler is to be wideband and more compact than the other microstrip balun types.

Basically, Marchand coupler consists of three microstrip lines whose electrical lengths are 90^0 and 180^0. A microstrip line with 180^0 of electrical length (half-wavelength) starts with un-balanced input and ends with open circuit. Two microstrip lines with 90^0 of electrical length (quarter-wavelength) start with balanced inputs and end with short circuit. Consequently, the single ended signal transforms to differential signals with the coupling between the microstrip line whose electrical length is 180^0 and two microstrip lines whose electrical lengths are 90^0 [41]. The operating principle of Marchand coupler is shown in Figure 3.1.

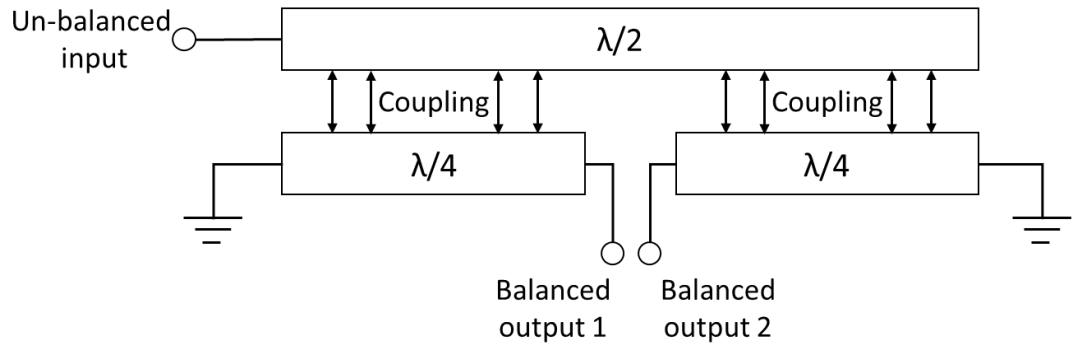

Figure 3.1: Operating principles of Marchand coupler

In this thesis, two Marchand couplers are designed for 2.4 GHz and 5.8 GHz of frequency. The difference between these couplers is their dimensions.

Marchand coupler operated at 2.4 GHz is designed and analyzed using HFSS. It is located on 1.6 mm thick FR4 material (ε_r=4.4, tangent loss=0.02) substrate. HFSS design of 2.4 GHz Marchand coupler can be seen in Figure 3.2 with its detailed dimensions.

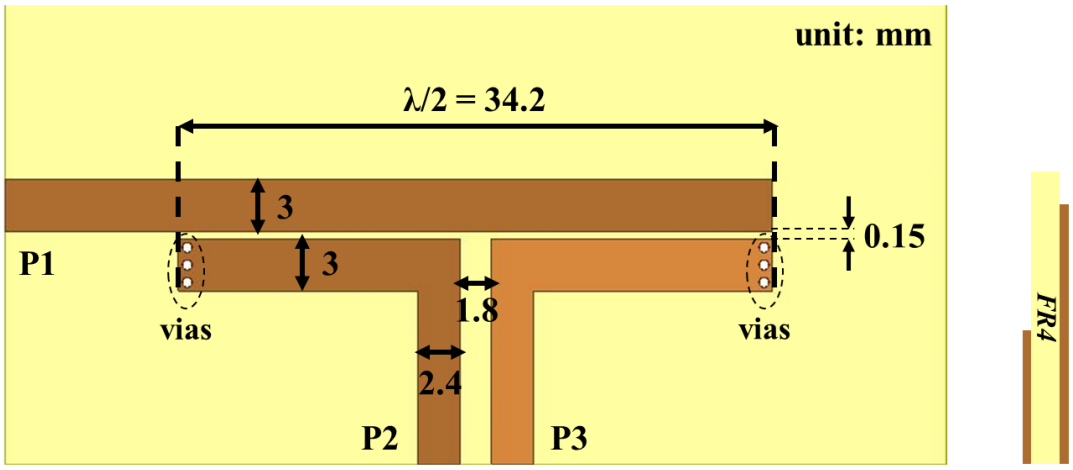

Figure 3.2: HFSS design of 2.4 GHz Marchand coupler

As shown in Figure 3.2, half-wavelength and quarter-wavelength microstrip lines have 50-ohm impedance, which corresponds to 3 mm width on 1.6 mm thick FR4 substrate. The physical separation between these lines is 0.15 mm, which is a small value for successful coupling. Output lines of Marchand coupler are set to 2.4 mm to achieve better return loss (S_{11}). To provide short circuit, vias are located to the end of quarter-wavelength microstrip lines. The mission of these vias is to create electrical connection to the ground plane, which is located at the bottom of FR4 substrate.

Simulated S-parameters results and phase difference between balanced output ports (S_{12} – S_{13} in degree) for Marchand coupler are shown in Figure 3.3. The designed Marchand coupler operates between 2 – 2.8 GHz with 180^0 of phase difference between P_2 and P_3.

Marchand coupler operated at 5.8 GHz also gives approximately same results. Its difference compared to 2.4 GHz Marchand coupler is its dimensions. Since wavelength at 5.8 GHz is smaller than 2.4 GHz, dimensions of this coupler are much smaller. In Figure 3.4, HFSS design of Marchand coupler for 5.8 GHz is shown with detailed dimensions.

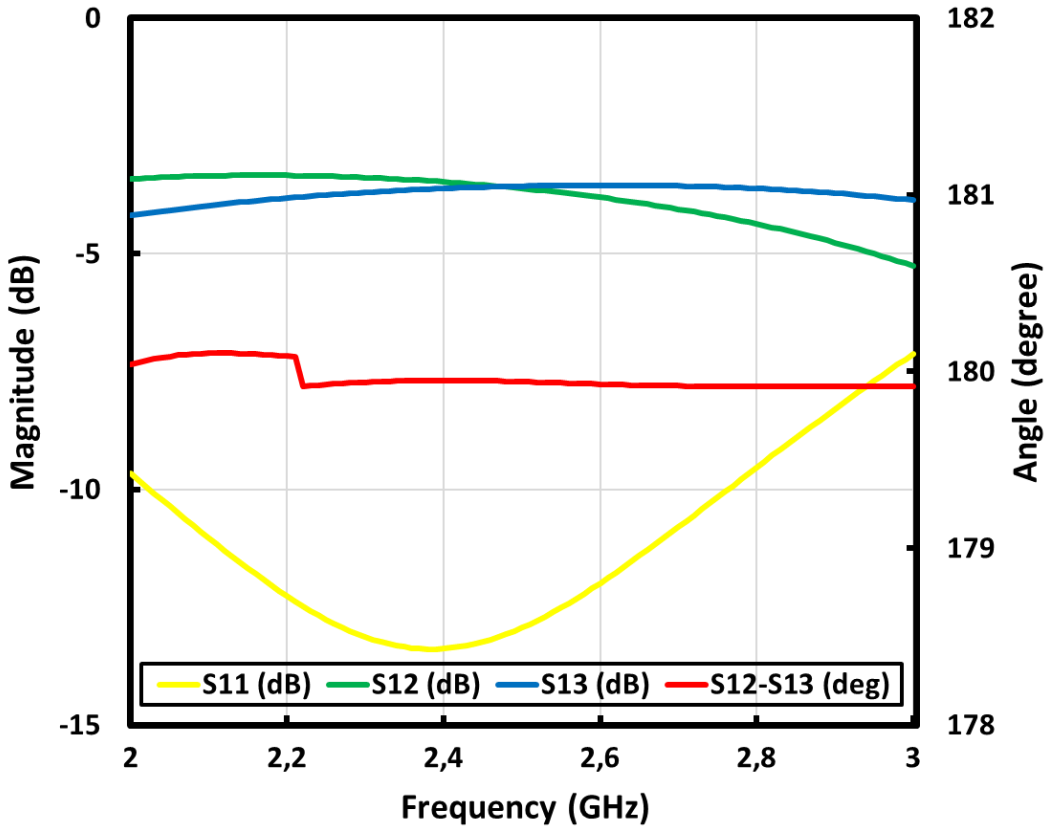

Figure 3.3: Simulated S-parameter (S_{11}, S_{12} and S_{13}) and phase difference ($S_{12} – S_{13}$) results

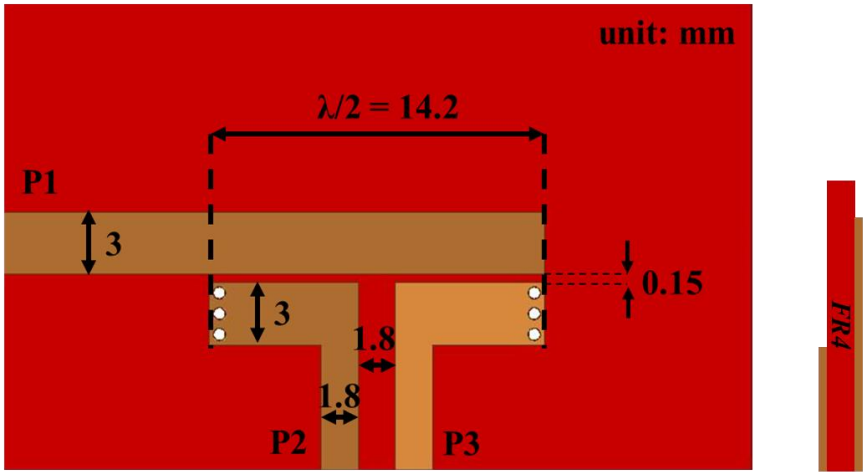

Figure 3.4: 5.8 GHz Marchand coupler

3.2. 2.4 GHz IBFD Differential Fed Microstrip Patch Antenna Array

The first one of the proposed antennas in this thesis is IBFD microstrip patch antenna array operated at 2.4 GHz. In [6], the similar work is presented using hybrid coupler as an external SI cancellation circuit. One of the advantages of this antenna compared to [6] is to be more compact and much smaller due to the usage of Marchand Coupler. The proposed antenna consists of two array elements and a Marchand coupler. Three port two elements microstrip patch antenna array and its S-parameters results can be seen in Figure 3.5(a) and Figure 3.5(b). Second array element is placed $\lambda_0/4$ away from the first array element where λ_0 corresponds to free space wavelength at 2.4 GHz. Return loss of ports of array elements (S_{11}, S_{22}, and S_{33}). It also shows $S_{12} - S_{13}$ operation, which is possible with feeding differential these ports.

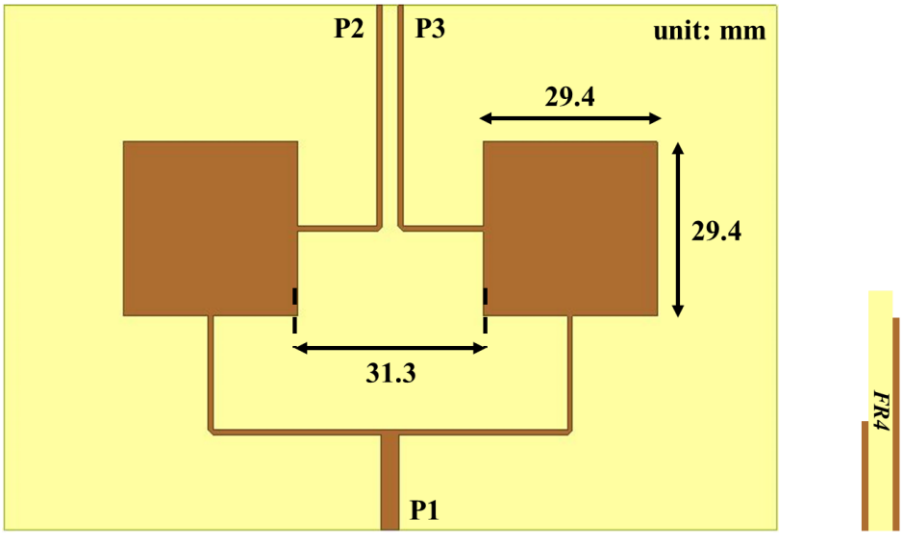

(a)

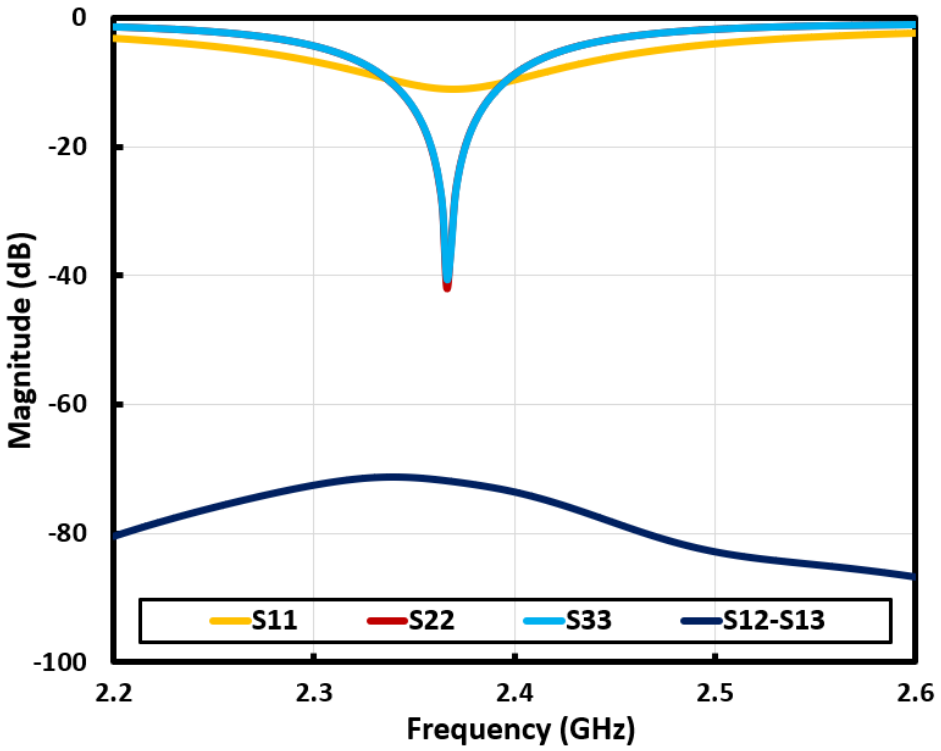

(b)

Figure 3.5: Three port two elements microstrip patch antenna array (a) HFSS design (b) Simulation results

To feed differential P_2 and P_3, Marchand coupler is used as an external SI cancellation circuit. HFSS design of 2.4 GHz IBFD microstrip patch antenna array included antenna array elements and Marchand coupler is shown in Figure 3.6(a). S-parameters results of this structure are shown in Figure 3.6(b). According to these results, the proposed antenna operates between 2.34 GHz – 2.4 GHz. Furthermore, the architecture obtains better than 55 dB of interport isolation (S_{12}) for 60 MHz antenna input bandwidth. Interport isolation at center frequency is more than 85 dB.

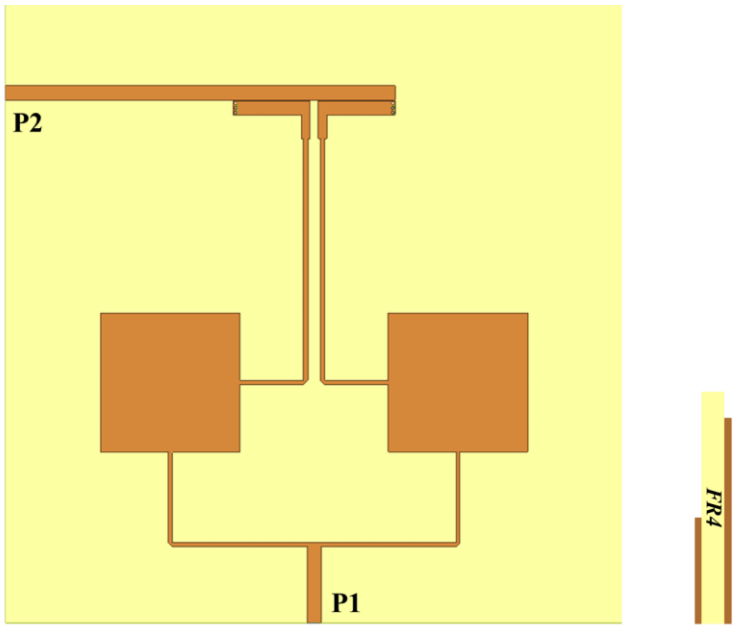

(a)

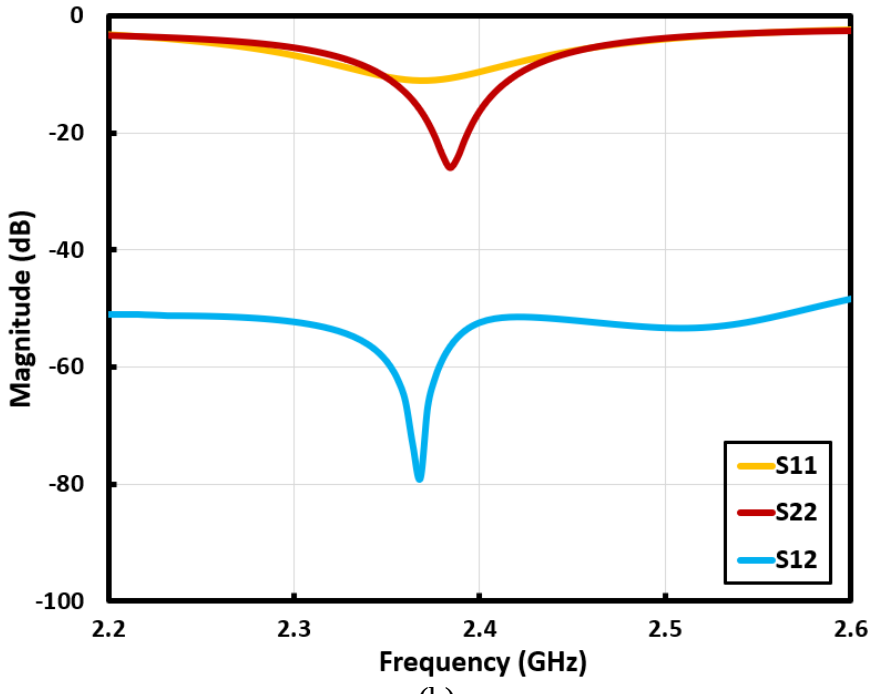

(b)

Figure 3.6: 2.4 GHz IBFD differential fed microstrip patch antenna array (a) HFSS design (b) S-parameters simulation results

The proposed antenna has a high gain because of the array setup. Figure 3.7(a) shows the simulated E-plane realized gain patterns for phi=0 and phi=90 of 2.4 GHz IBFD microstrip patch antenna array. At 2.4 GHz, its peak realized gain is 4.56 dBi.

The simulated co-polarization and cross-polarization gain results for the designed IBFD microstrip patch antenna array are seen in Figure 3.7(b). It frankly shows that antenna has very low cross-polarization level, that causes a nice polarization purity.

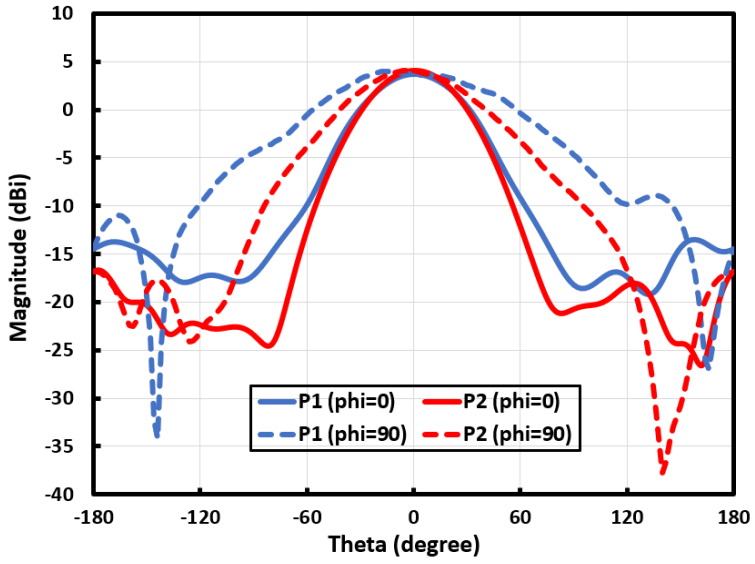

(a)

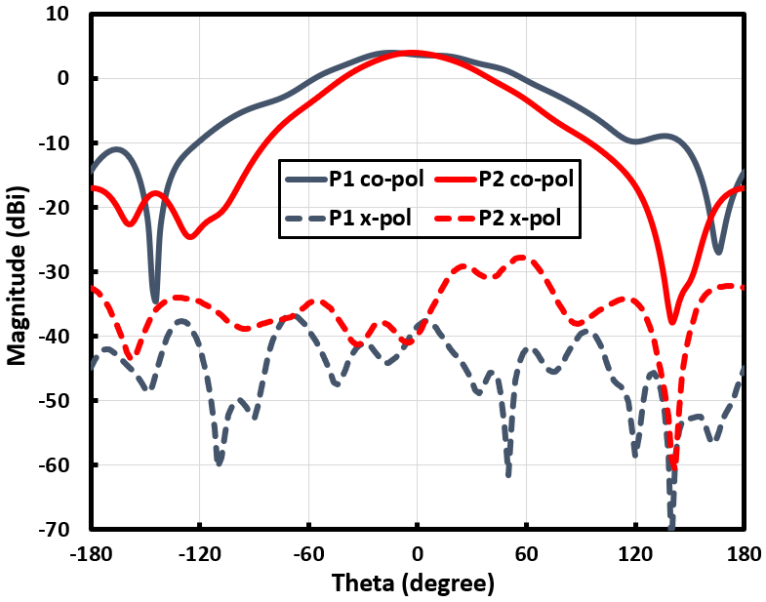

(b)

Figure 3.7: 2.4 GHz IBFD differential fed microstrip patch antenna array (a) Simulated E-plane realized gain patterns for phi=0 and phi=90 (b) Simulated co-pol and x-pol gain results

The designed antenna can be fabricated by etching Marchand coupler and array elements on the same side of 1.6 mm thick FR4 substrate with bottom layer of PCB as a ground plane.

3.3. 5.8 GHz IBFD Differential Fed Microstrip Patch Antenna Array

The proposed microstrip patch antenna array design consists of two parts: two array elements and Marchand coupler as an external SI cancellation circuit. HFSS design and simulation details of two elements array are shown in Figure 3.8. The physical separation between two elements is $\lambda_0/4$ where λ_0 corresponds to free space wavelength at 5.8 GHz. In Figure 3.5(b), return loss of ports of array elements (S_{11}, S_{22}, and S_{33}) and cancellation ($S_{12} - S_{13}$) of RF leakages from P_1 to P_2 (S_{12}) and P_1 to P_3 (S_{13}). $S_{12} - S_{13}$ operation can be performed by feeding differential these ports. Marchand coupler gets involved at this stage.

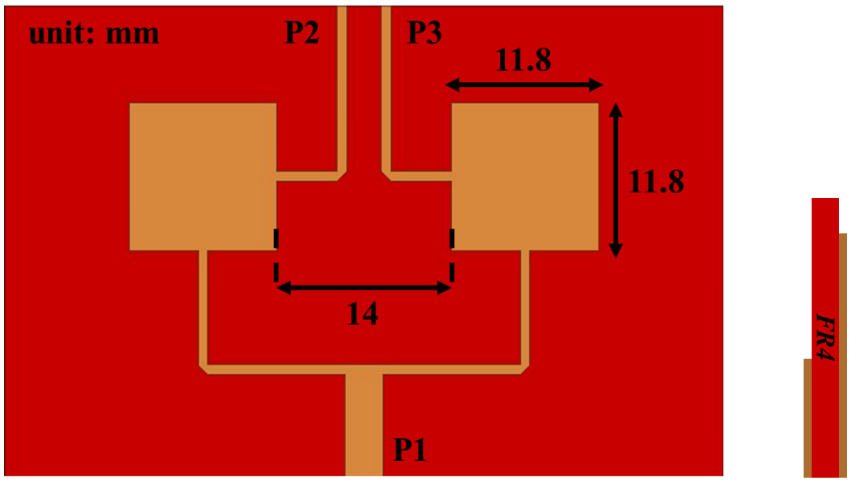

(a)

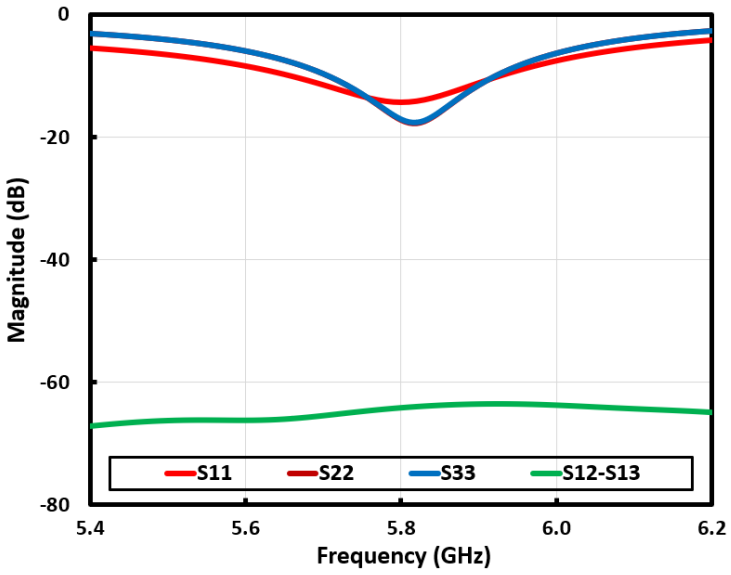

(b)

Figure 3.8: Three port two elements microstrip patch antenna array (a) HFSS design of array elements (b) Simulation results

An external Marchand coupler is connected to P_2 and P_3 to feed these ports differentially. IBFD microstrip patch antenna array design is seen in Figure 3.9(a). simulation results of return loss (S_{11} and S_{22}) and isolation between P_1 and P_2 (S_{12}) are shown in Figure 3.9(b). These results show that more than 83 dB of interport isolation is provided for the center frequency. Designed microstrip patch antenna array also provides higher than 50 dB of interport isolation over 200 MHz antenna input bandwidth. It operates between 5.7 GHz and 5.8 GHz.

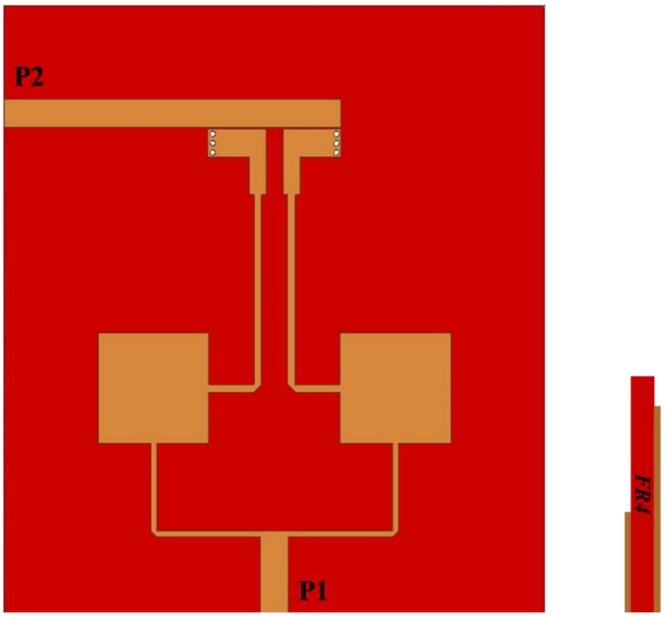

(a)

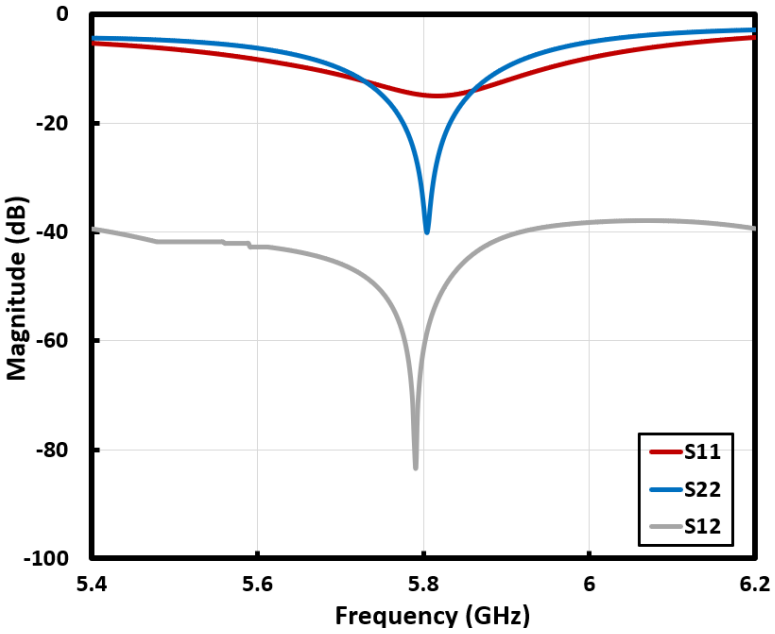

(b)

Figure 3.9: 5.8 GHz IBFD differential fed microstrip patch antenna array (a) HFSS design (b) Simulation results of S-parameters

Due to the array setup, the designed antenna provides high gain. Simulation results of peak realized gain versus frequency is shown in Figure 3.10(a). The peak realized gain changes from 5.1 dBi to 6.8 dBi for 200 MHz antenna input bandwidth (5.7 GHz – 5.9 GHz), when the antenna is fed from P_1 and P_2.

The simulated co-polarization and cross-polarization gain results of 5.8 GHz IBFD microstrip patch antenna array seen in Figure 3.10(b) clearly indicate that the antenna provides too low cross-polarization when it is fed from P_1 and P_2. Therefore, a perfect polarization purity is obtained by this structure.

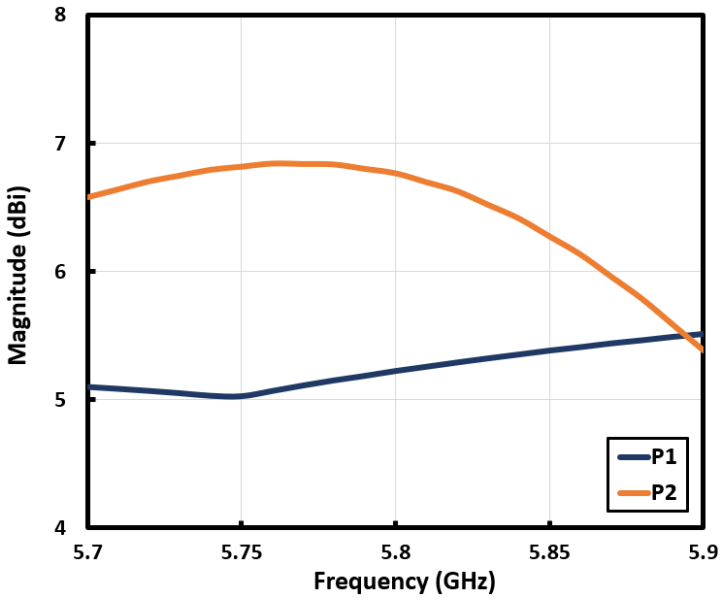

(a)

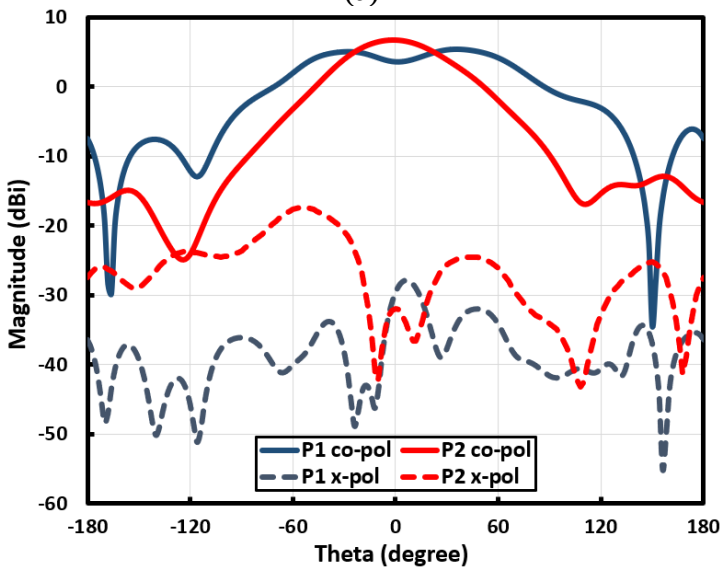

(b)

Figure 3.10: 5.8 GHz IBFD differential fed microstrip patch antenna array (a) Simulation results of peak realized gain (b) Simulation results of co-pol and x-pol

The designed structure can be fabricated by etching Marchand coupler and array elements at the same layer of 1.6 mm thick FR4 material with bottom side as ground plane.

3.4. 2.4 GHz IBFD Double Differential Fed Microstrip Patch Antenna

An external SI cancellation circuit has been used for feeding transmit/receive port differentially for proposed antennas in section 3.2 and section 3.3. In this design, the proposed antenna is differentially fed from both receive and transmit ports, in order to increase interport isolation.

2.4 GHz IBFD double differential fed microstrip patch antenna consists of a four-port radiating element and two Marchand couplers as SI cancellation circuits. In Figure 3.11(a), four-port radiating element with thin λ/4 feeds is shown. Double differential feeding network can be achieved by connecting P_1 and P_3 to an external differentiation circuit, while P_2 and P_4 are connected to another external differentiation circuit. S-parameters simulation results of four port radiating element are shown in Figure 3.11(b). The RF leakage from P_1 to P_2 and P_4 (S_{12} and S_{14}) interfere to cancel each other ($S_{12} – S_{14}$). This operation is performed in order to differential excitation of P_2 and P_4. Similarly, it is performed at P_3, and $S_{32} – S_{34}$ is gotten. With combination of these operations, ($S_{12} – S_{14}$) – ($S_{32} – S_{34}$) gives the total SI cancellation.

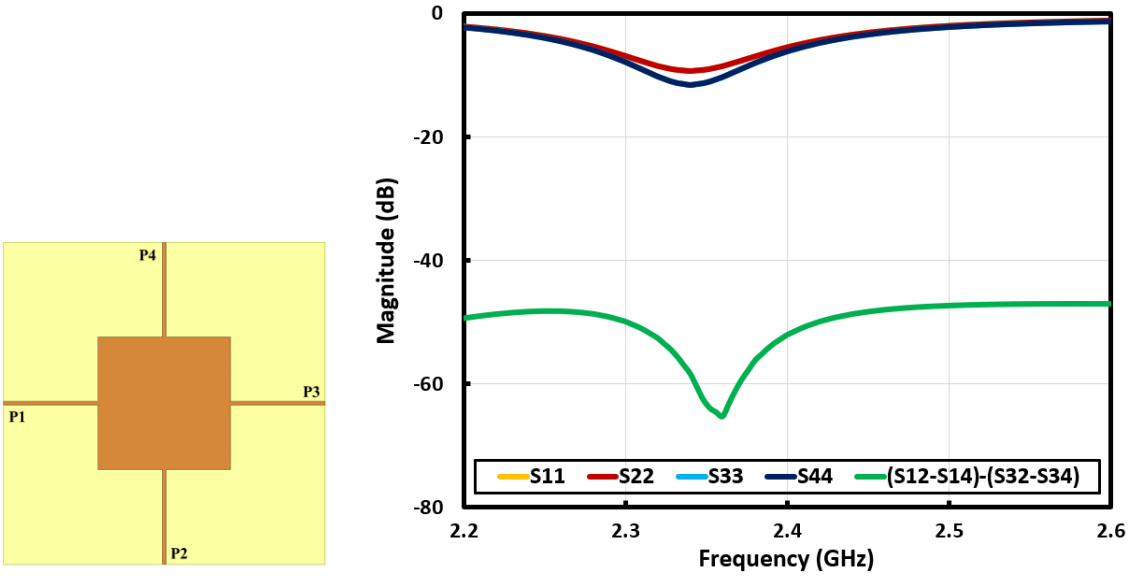

(a) (b)

Figure 3.11: Four-port radiating element (a) HFSS design of four port radiating element (b) S-parameters results

($S_{12} - S_{14}$) – ($S_{32} - S_{34}$) operation can be performed by connecting differentiation circuits between P_1 and P_3 with P_2 and P_4. Again, Marchand coupler is used as an SI cancellation circuit. HFSS design of 2.4 GHz microstrip patch antenna can be seen in Figure 3.12. A Marchand coupler connects to four-port radiating element with microstrip lines, that is seen in Figure 3.12(a). The other Marchand coupler locates at different substrate, which is located at the bottom of first substrate, as it is seen in Figure 3.12(b). The cross-sectional view of the designed antenna can be seen in Figure 3.12(c).

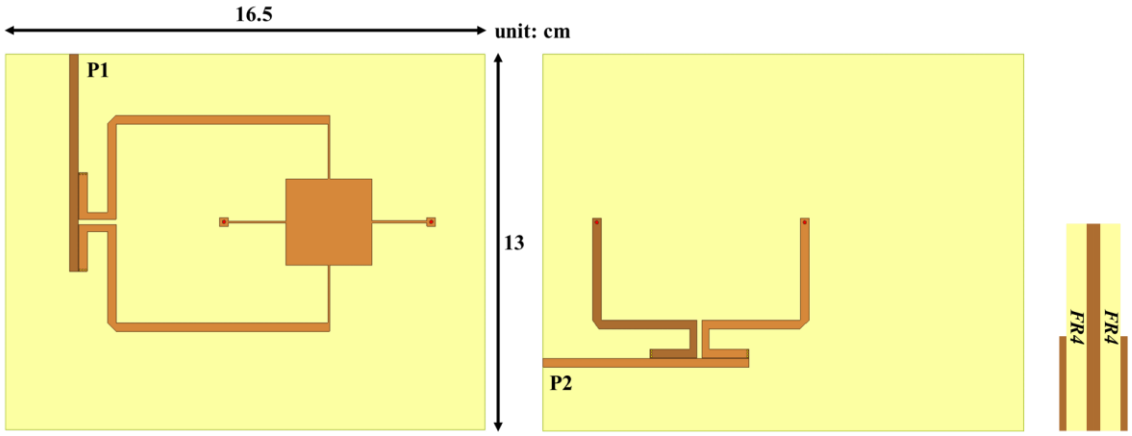

(a) (b) (c)

Figure 3.12: Design of 2.4 GHz IBFD double differential fed microstrip patch antenna (a) Top layer (b) Bottom layer (c) Cross-sectional view

Figure 3.13 shows the S-parameters simulation results of the proposed antenna. It ensures interport isolation of higher than 70 dB for its 10 dB input bandwidth (between 2.32 and 2.38 GHz). Furthermore, it provides better than 80 dB of interport isolation for 30 MHz. In addition, higher than 85 dB of peak interport isolation is obtained.

Keysight Advanced Design System (ADS) [42] simulated surface currents of the proposed antenna when it is excited from P_1 and P_2 can be seen in Figure 3.14. In case it is fed from P_1, it seems as horizontally polarized and if it is fed from P_2, vertical polarization is provided. Therefore, one can comment that the designed antenna is dual-polarized.

The proposed architecture consists of two FR4 substrates. First substrate has Marchand coupler and four-port radiating element. Second one has only Marchand coupler. The

electrical connection between second Marchand coupler and four-port radiating element is created by very thin copper wires.

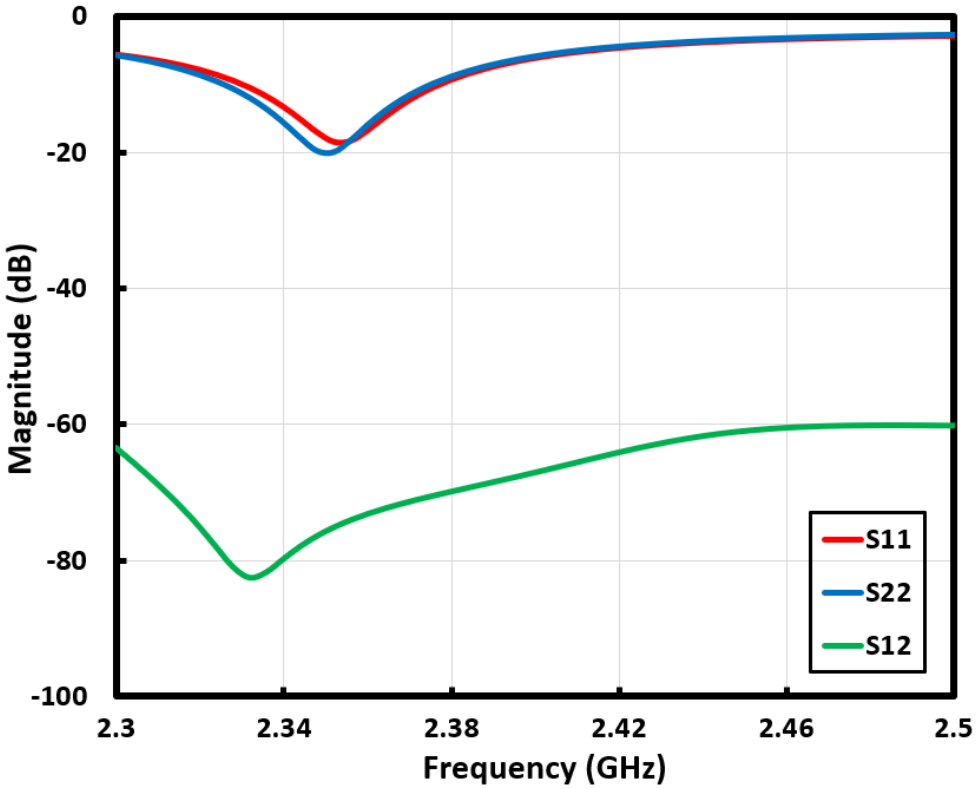

Figure 3.13: S-parameters simulation results of 2.4 GHz IBFD double differential fed microstrip patch antenna

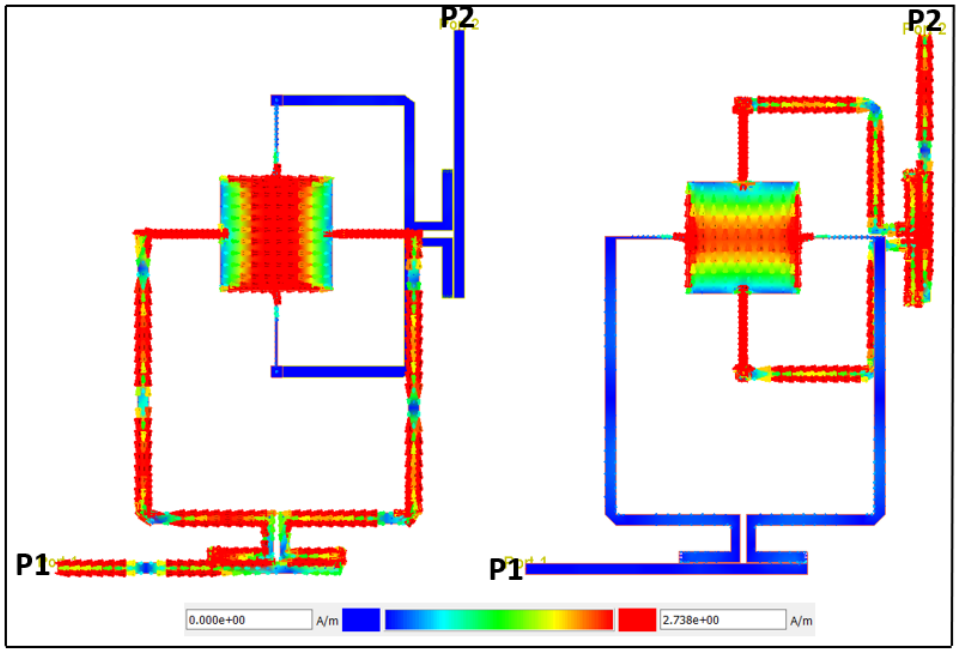

Figure 3.14: ADS Momentum simulated surface currents of 2.4 GHz IBFD double differential fed microstrip patch antenna

3.5. 3.6 GHz Double Differential Fed Microstrip Patch Antenna

The designed antenna discussed in previous section is modified to 3.6 GHz version. Differently from other reported IBFD microstrip patch antennas, to achieve better return loss bandwidth, the substrate is selected as 1.52 mm thick Rogers RO4003 (ε_r=3.38, tangent loss=0.0027) since it is less lossy than FR-4 substrate.

As can be seen in Figure 3.15, 3.6 GHz double differential fed patch antenna has a more compact structure than 2.4 GHz version because of its smaller dimensions. As known, the length of the microstrip line is inversely proportional to the dielectric constant of substrate, however, it is directly proportional to operating frequency. Since the operating frequency band of the designed antenna is higher than its 2.4 GHz version, the more compact antenna is achieved.

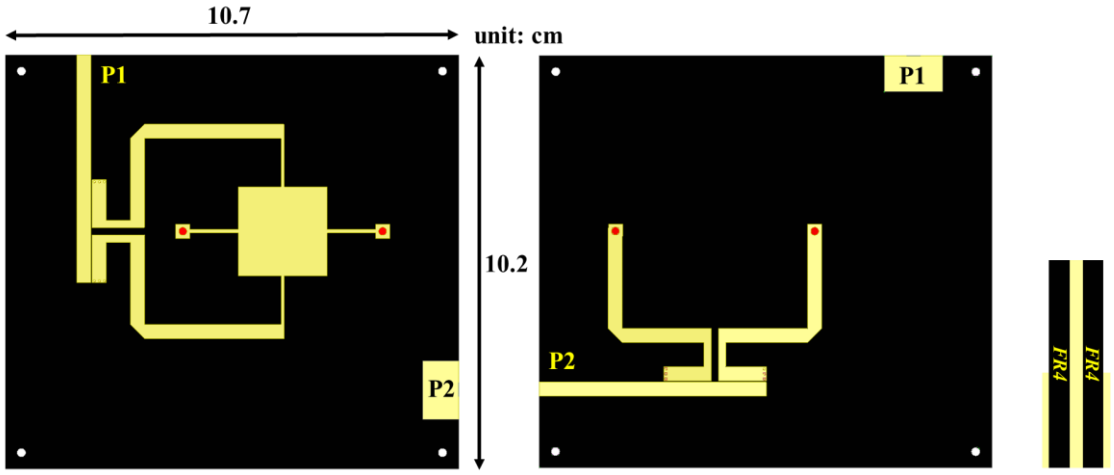

(a) (b) (c)

Figure 3.15: (a) Top layer (b) bottom layer and (c) cross-sectional view of designed 3.6 GHz double differential fed antenna

Simulated return loss (S_{11} and S_{22}) and the isolation between P_1 and P_2 (S_{12}) results seen in Figure 3.16(a) shown the antenna operates between 3.63 – 3.68 GHz. Moreover, it provides higher than 40 dB over antenna input bandwidth of 50 MHz. Simulated peak realized gain at 3.6 GHz frequency shows the antenna provides gain of 1-5 dBi in case phi = 0 and phi = 90 degrees, as it can be seen in Figure 3.16(b).

As its 2.4 GHz version, the designed 3.6 GHz double differential fed patch antenna can be fabricated as two different FR4 substrates. After, these substrates can be stacked to each other with screws.

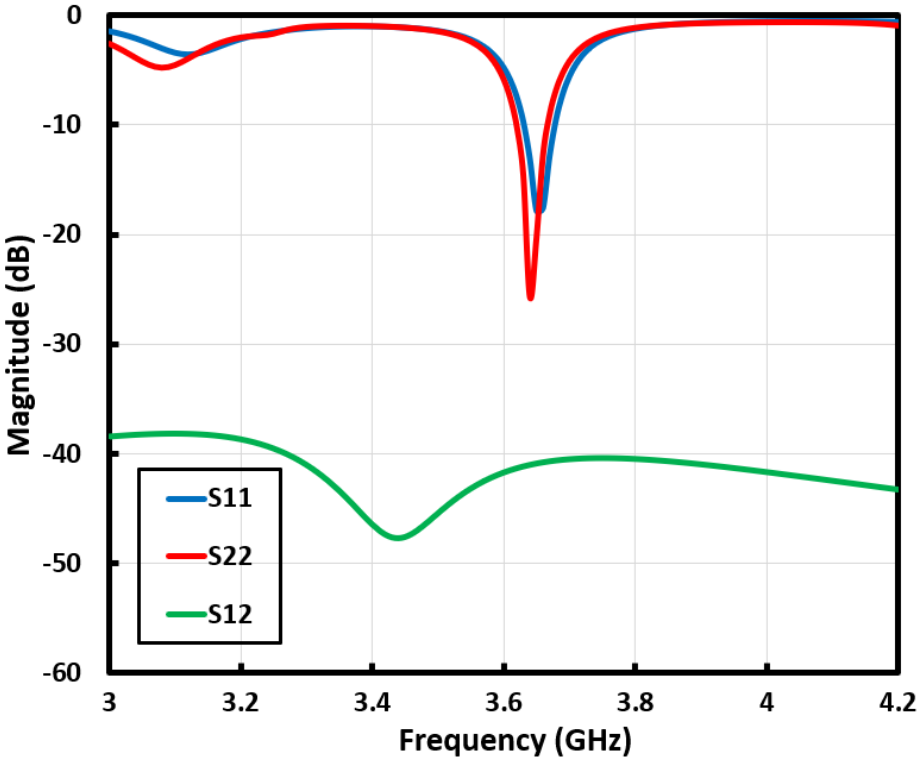

(a)

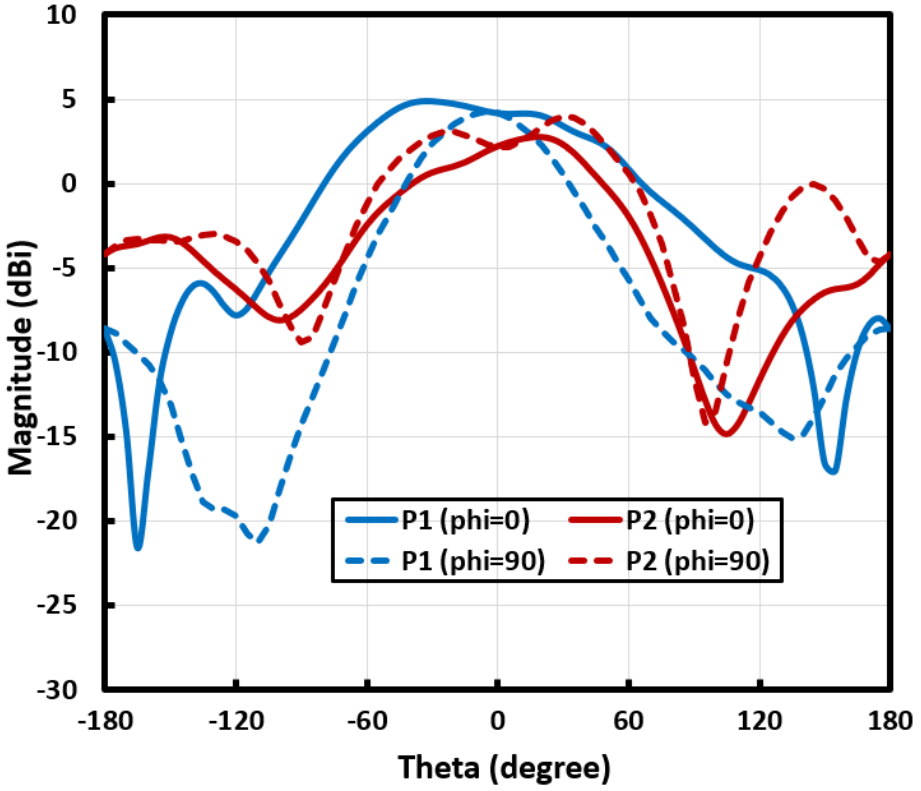

(b)

Figure 3.16: HFSS simulation results of 3.6 GHz antenna (a) S-parameters (b) Peak realized gain at 3.6 GHz

4. MEASUREMENT DETAILS OF PROPOSED IBFD MICROSTRIP PATCH ANTENNAS

In this chapter, the measurement details of proposed antennas discussed in chapter 3 are introduced. These antennas have been fabricated by etching technique on 1.6 mm thick FR4 material (ε_r=4.4 and tangent loss=0.02) with the other side of PCB as a ground plane. 2.4 GHz IBFD differential fed microstrip patch antenna array and double differential fed microstrip patch antenna have been fabricated in Turkey, while 5.8 GHz IBFD differential fed microstrip patch antenna array has been fabricated in China. Since we are not convinced by the provided return loss bandwidth of 3.6 GHz double differential fed microstrip patch antenna, it has not been fabricated. This chapter consists of three sections:

(vi) Measurement details of 2.4 GHz IBFD differential fed microstrip patch antenna array

(vii) Measurement details of 5.8 GHz IBFD differential fed microstrip patch antenna array

(viii) Measurement details of 2.4 GHz IBFD double differential fed microstrip patch antenna

4.1. 2.4 GHz IBFD Differential Fed Microstrip Patch Antenna Array

The design details and simulation analysis of 2.4 GHz IBFD differential fed microstrip patch antenna array have been discussed in section 3.2. Fabricated antenna is seen in Figure 4.1. It has two ports; one for transmit RF signal and one for receive RF signal. Since it transmits and receives RF signals simultaneously, it is called as transceiver. The antenna has an area of 169 cm^2. There are 6 vias on Marchand coupler due to create short circuits at the end of balanced outputs.

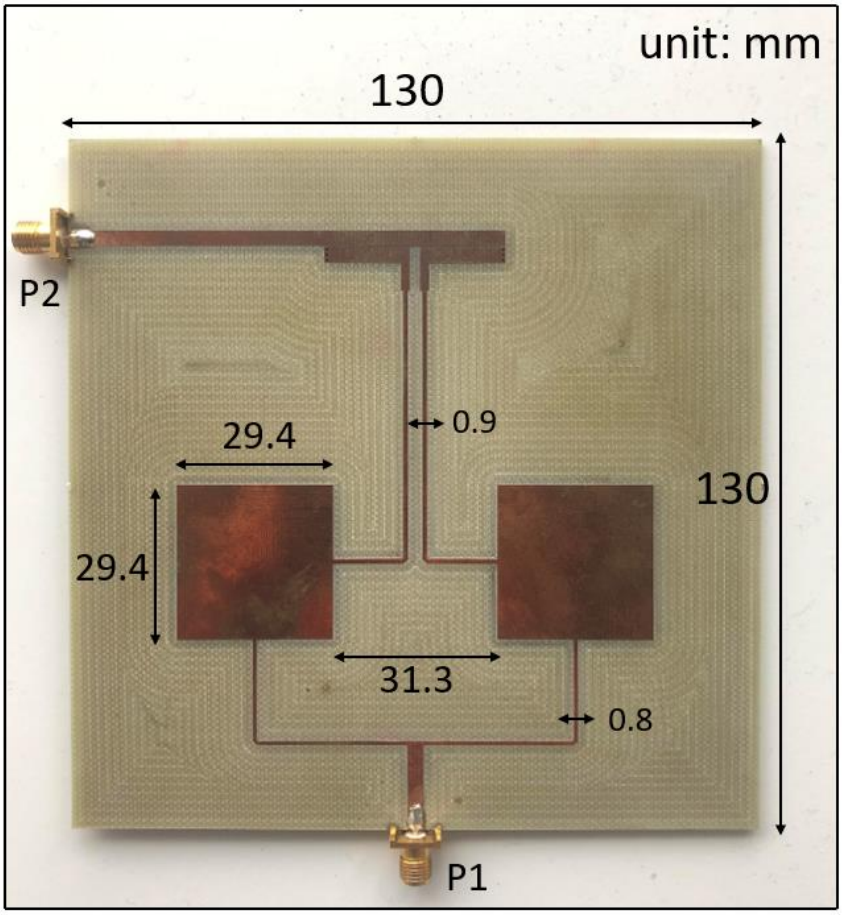

Figure 4.1: Fabricated 2.4 GHz IBFD differential fed microstrip patch antenna array

The distance between elements is $\lambda_0/4$ where λ_0 corresponds to free space wavelength at 2.4 GHz. Thin feed lines with 0.8 mm and 0.9 mm of thickness are used for impedance matching. Marchand coupler which has been presented in section 3.1 is used as a differential feeding network.

Measurements were performed at Sabancı University RF/Wireless Laboratory. Keysight E5062A Network Analyzer [43] is was used to perform measurements of return loss (S_{11} and S_{22}) and isolation between P_1 and P_2 (S_{12}). Ports of network analyzer were calibrated with the help of Keysight 85032E calibration kit [44]. The simulation and measurement results of S-parameters are shown in Figure 4.2. The fabricated antenna obtains better than 53 dB of interport isolation for antenna's 10 dB return loss bandwidth (2.38 GHz – 2.43 GHz). Moreover, the peak isolation value of the fabricated antenna is more than 65 dB. As clearly seen, one can comment that the simulation and measurement results match to each other.

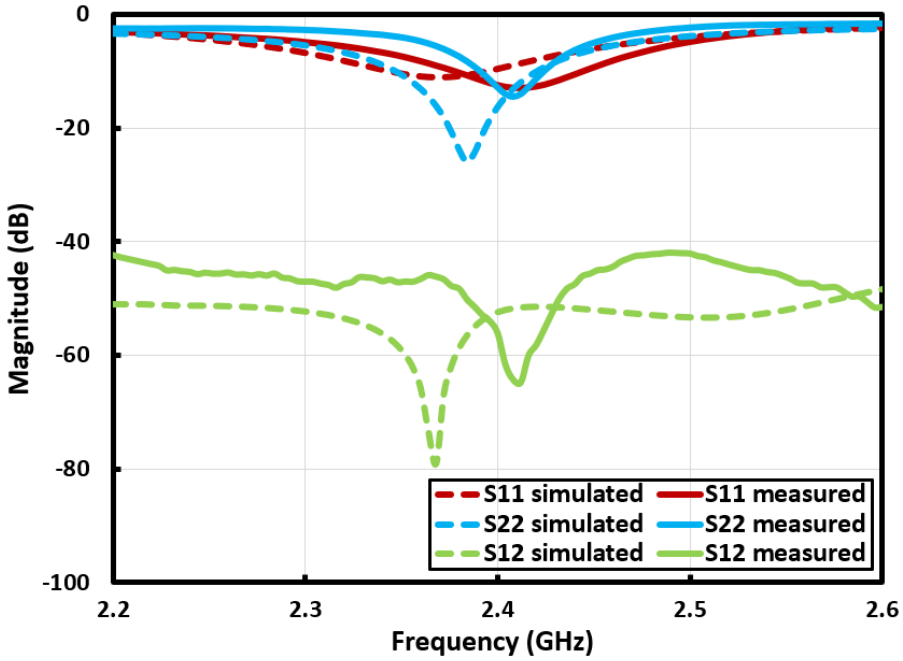

Figure 4.2: S-parameters simulation and measurement results of 2.4 GHz IBFD differential fed microstrip patch antenna array

The measured return loss (S_{11} and S_{22}) and isolation between P_1 and P_2 (S_{12}) show that there is a frequency shift to the right side in comparison with simulated ones since the dielectric constant of FR4 substrate can be changed from 4.2 to 4.6, in real life. HFSS simulations are performed considering dielectric constant as 4.4, however, Figure 4.3 shows that frequency shifts to right in case the dielectric constant of substrate decreases. According to these results, the dielectric constant of fabricated FR4 substrate can be determined as between 4.2 and 4.4.

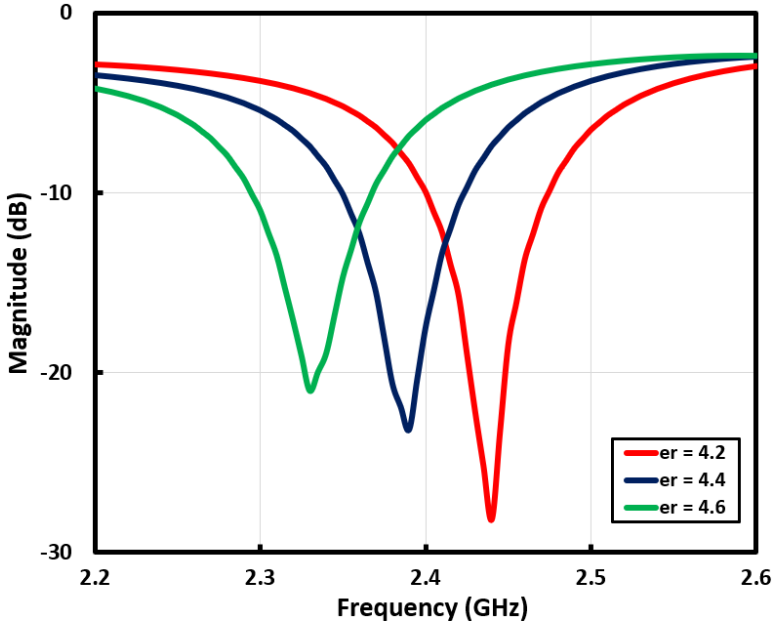

Figure 4.3: The effect of the dielectric constant to return loss

4.2. 5.8 GHz IBFD Differential Fed Microstrip Patch Antenna Array

The design details and simulation analysis of 5.8 GHz IBFD differential fed microstrip patch antenna array discussed in section 3.3 was fabricated in China. The fabricated antenna is shown in Figure 4.4. Similar to the previous antenna, it consists of two ports, one receives RF signal and the other one transmits RF signal. Transmitting and receiving are realized simultaneously. Since free space wavelength decreases at higher frequencies, dimensions of this antenna are smaller than one half of 2.4 GHz IBFD differential fed microstrip patch antenna array. The fabricated antenna has an area of 37.2 cm^2, that brings a more compact view. Red color areas represent solder mask that protects substrate from solder. It also prevents the copper layer from oxidation. There are solder mask openings at vias located areas due to block leaking. 5.8 GHz IBFD differential fed microstrip patch antenna array was fabricated using 1.6 mm thick FR4 material.

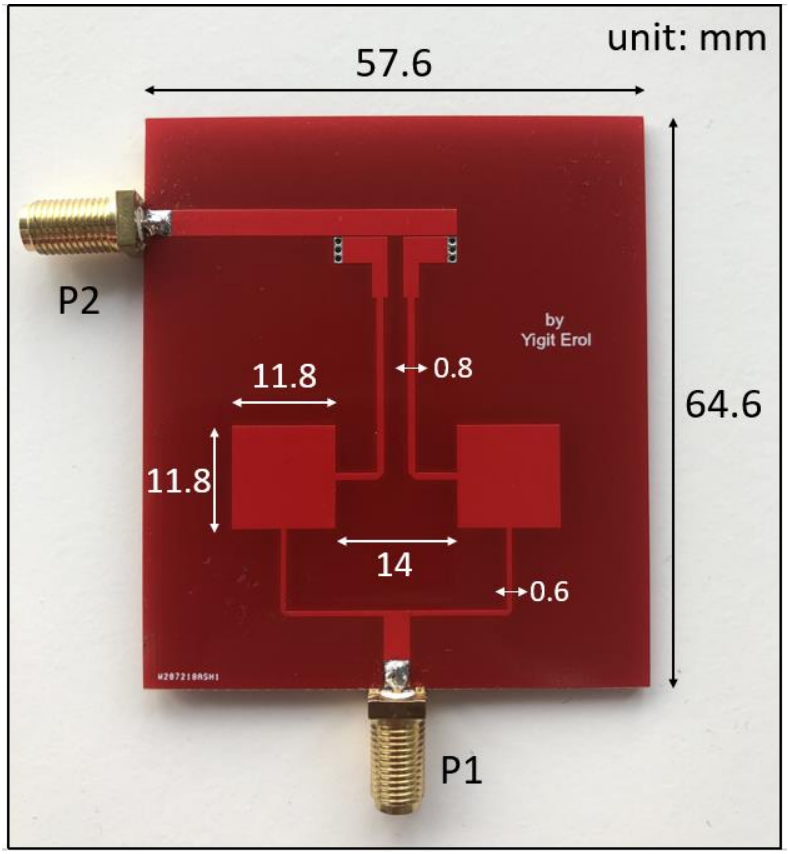

Figure 4.4: Fabricated 5.8 GHz IBFD differential fed microstrip patch antenna array

The separation between elements is $\lambda_0/4$, where λ_0 presents free space wavelength at the specified frequency. The array elements are fed with thin feed lines for impedance matching. The dimensions of Marchand coupler are also decreased because of the increment of operating frequency.

S-parameters measurements were performed at Istanbul Technical University RF Electronic Laboratory [45] with Rohde & Schwarz FSH8 Network Analyzer [46]. SOLT (short, open, load, thru) calibration was completed with Rohde & Schwarz ZV-Z135 Calibration Kit [47]. The fabricated antenna achieves higher than 51 dB of interport isolation for the fabricated antenna's 10 dB input bandwidth (5.78 GHz – 5.98 GHz), as seen in Figure 4.5. Since the operating frequency is increased, this antenna operates at 200 MHz bandwidth, that is four times of operating bandwidth of 2.4 GHz differential fed microstrip patch antenna. Furthermore, more than 60 dB of interport isolation is provided for 60 MHz of bandwidth (5.84 GHz – 5.9 GHz). The peak interport isolation of the fabricated antenna is more than 77 dB. Simulation and measurement results are close to each other, clearly.

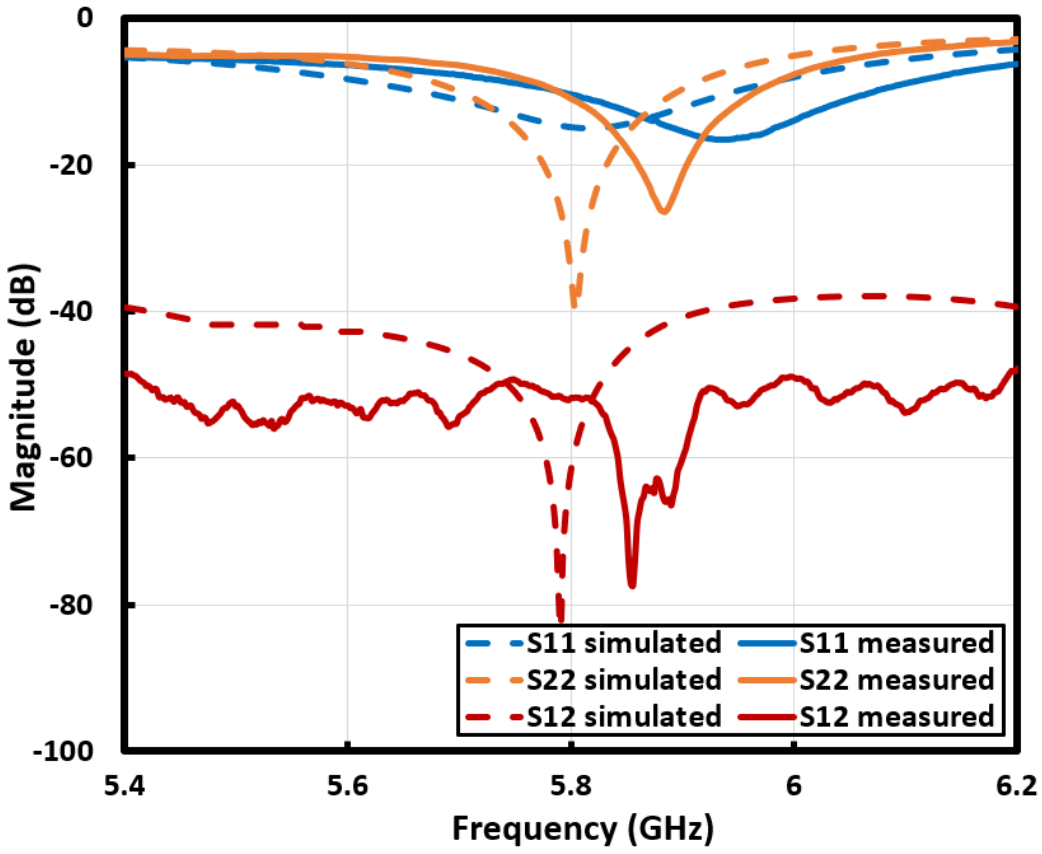

Figure 4.5: S-parameters simulation and measurement results of 5.8 GHz IBFD differential fed microstrip patch antenna array

4.3. 2.4 GHz IBFD Double Differential Fed Microstrip Patch Antenna

The design details and simulation results of 2.4 GHz IBFD microstrip patch antenna has been presented in section 4.4. The fabricated antenna and its dimensions seen in Figure 4.6 consists of two ports, one of these transmits RF signal and the other one receives RF signal, simultaneously. The implemented antenna consists of two FR4 substrates whose thickness are 1.6 mm. At the top layer of the first substrate, Marchand coupler and four-port radiating element have been etched. The other side of the top substrate is the ground plane. Only Marchand coupler is etched at the top layer of the bottom substrate which has the ground plane at the bottom layer. The electrical connection between 4 port radiating element and Marchand coupler located at the second substrate is provided by 0.1 mm thick copper wire. Copper wire has been soldered to top layers of first and second substrates. The antenna architecture has an area of 214 cm^2.

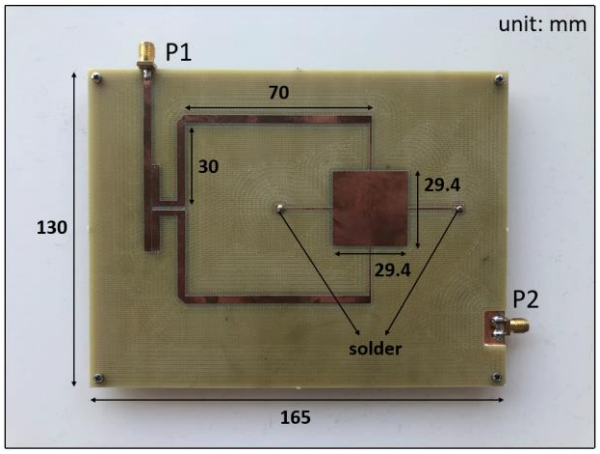

(a)

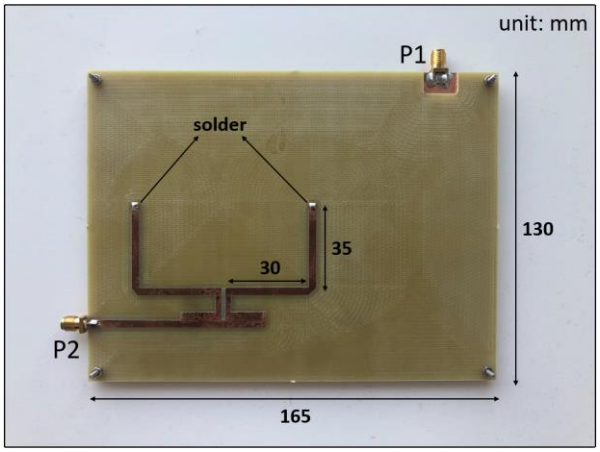

(b)

Figure 4.6: 2.4 GHz IBFD double differential fed microstrip patch antenna (a) The top layer of first substrate (b) The top layer of second substrate

S-parameters measurements were performed at Sabancı University RF Wireless Laboratory with Keysight E5062A Network Analyzer. The network analyzer was calibrated with the help of Keysight 85032E calibration kit.

As shown in Figure 4.7, the implemented antenna provides more than 62 dB over its input bandwidth (2.35 GHz – 2.40 GHz). Furthermore, the peak isolation provided by the antenna is more than 79 dB. Simulation and measurement results are very close to each other as it is shown in Figure 4.7.

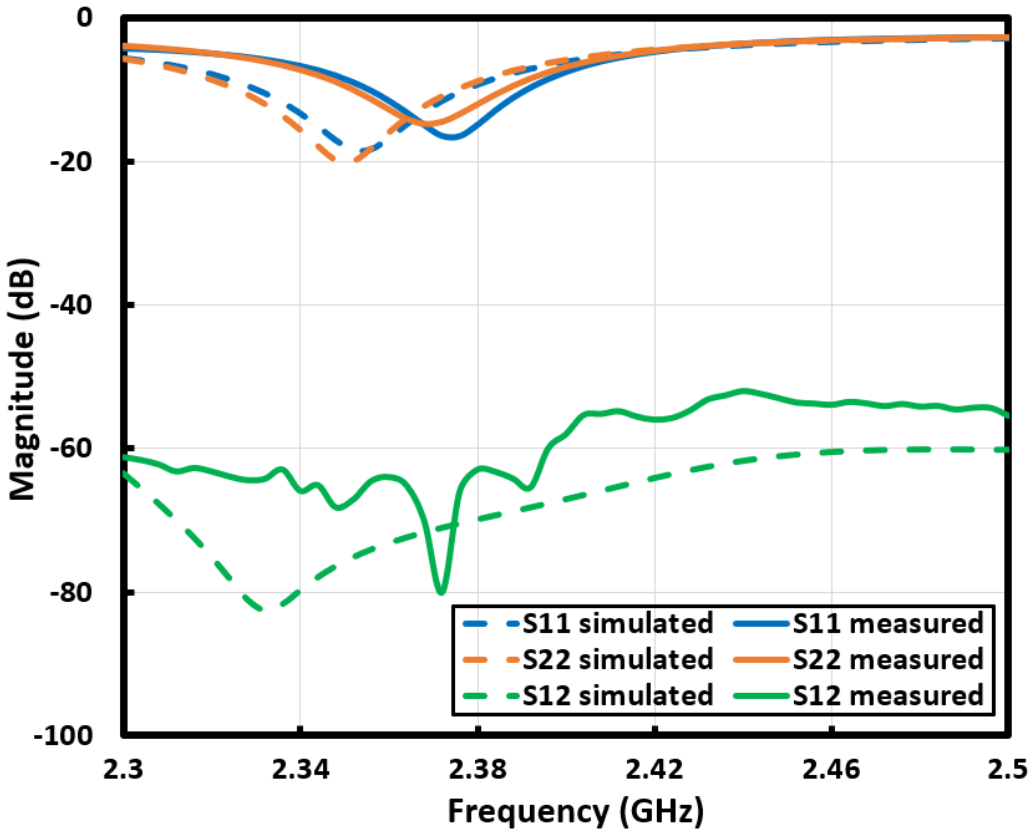

Figure 4.7: S-parameters simulation and measurement results of 2.4 GHz IBFD double differential fed microstrip patch antenna

5. UWB IBFD ANTENNA

In this chapter, the design details, implementation, and measurements of the UWB IBFD antenna are presented. The difference of the UWB IBFD antenna compared to the other reported microstrip patch antennas is to have a wide return loss bandwidth with a reasonable interport isolation. The antenna consists of a 3-port radiating element with a UWB balun in order to create differential feeding network. High Frequency Structure Simulator (HFSS) [39] is used for the design and simulation analysis of the proposed antenna. Rogers RT/Duroid 5880 (ε_r=2.2, tangent loss=0.0009) is preferred as a substrate due to its low-loss material. This chapter consists of two main sections:

(i) Design details and simulation analysis of 3-port radiating element and UWB balun

(ii) Design details and simulation analysis of UWB IBFD antenna

(iii) Fabrication and measurement details of the UWB IBFD antenna

5.1. Design Details and Simulation Analysis of 3-Port Radiating Element and UWB Balun

The proposed UWB IBFD antenna is configured based on 3-port radiating element with a UWB balun in order to form the differential feeding network. Since Marchand coupler presented in previous chapters do not have a wide operation bandwidth, a different balun with a wider bandwidth is required. This section presents design details and simulation analysis of 3-port radiating element and the UWB balun with two different parts.

5.1.1. UWB Balun

In order that implement UWB IBFD antenna, a UWB balun is necessary. One of the best advantages of balun reported in [48] is to be a very compact structure with small dimensions in addition to its wide operation bandwidth. It can be divided as three microstrip lines and a slotline at ground plane. The signal fed from P_1 can reach to P_2 and P_3 by the help of Microstrip to Slotline Transition Forms I and II (MSI and MSII).

When a signal feeds P_1, it is transmitted to the slotline via MSI. MSI is performed by a conductor via with diameter of lv. Because of the symmetrical structure, the input signal divides into two identical signals after it reaches to the slotline. Herewith, these two signals come to output microstrip lines through MSII. MSII is carried out by electromagnetic coupling between slotline and microstrip lines. Note that the direction of open circuit (O.C.) sides of output microstrip lines are opposite to each other, thus, the phase of output signals will be opposite to each other. As a result, the input signal fed from P_1 is divided into two equal output signals at P_2 and P_3, with 180^0 of phase difference. The bottom view of the designed UWB balun and its dimensions are shown in Figure 5.1.

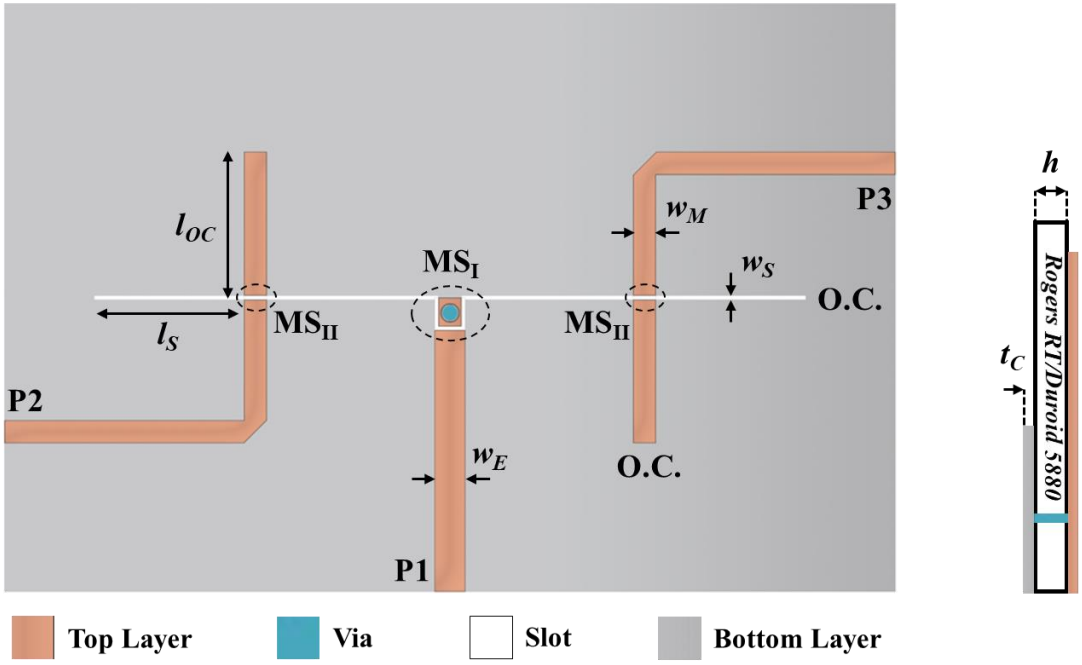

Figure 5.1: The bottom view of the designed UWB balun

Impedance matching and operating frequency range of designed UWB balun are optimized by tuning its dimensions. The impedance of microstrip lines and slotline should be 50 Ω in theory. Nevertheless, the slotline impedance is chosen as 80 Ω due to fabrication limitation. After parametric simulations done in HSSS, the impedance of output microstrip lines are selected as 57 Ω, while inputs are still as 50 Ω. The lengths of output microstrip lines and slotline in O.C. sides are quarter wavelength ($\lambda_0/4$) at 4.5 GHz since they manage the center frequency of operating bandwidth of balun. The dimensions of optimized balun are shown in Table 5.1.

Table 5.1: The dimensions of the designed UWB balun

Symbol	Dimension
w_E	2.4
w_M	2.2
w_s	0.1
l_{oc}	12.6
l_s	11.4
l_v	1.4
w_E	2.4
t_C	0.035
h	0.79

unit: mm

The designed UWB balun is simulated with high mesh number to reach to high accuracy. As can be seen in Figure 5.2, simulation results show that designed UWB balun achieves 5.46 GHz (between 2.04 and 7.50 GHz) of 10 dB return loss bandwidth, and its simulated insertion loss is less than 1.6 dB over its operation bandwidth. In addition, it can be clearly seen that $180^0 \pm 0.5^0$ of phase difference between P_2 and P_3 is achieved.

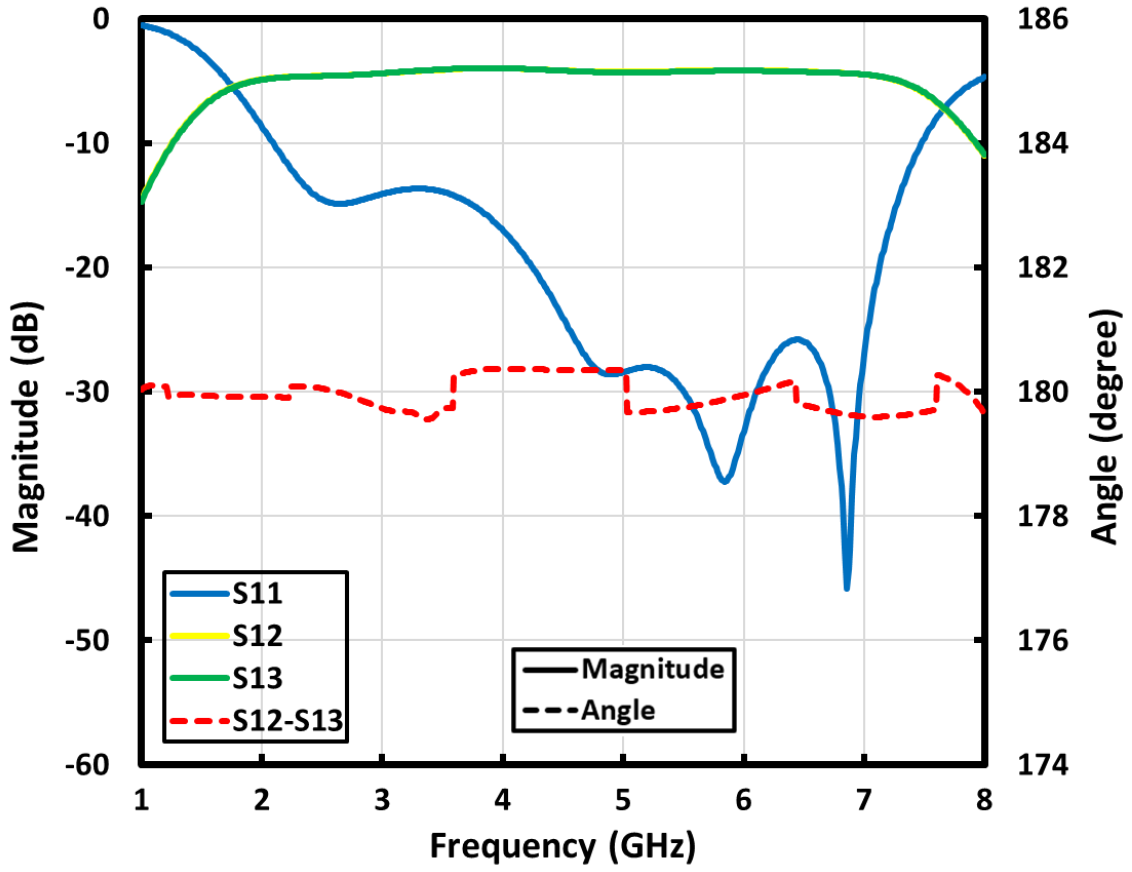

Figure 5.2: Simulated return loss (S_{11}), insertion loss (S_{12} and S_{13}) and phase difference between P_2 and P_3 ($S_{12} - S_{13}$)

5.1.2. 3-Port Radiating Element

In this section, the design and simulation process of three ports radiating element is presented. 3-port radiating element was inspired by the planar monopole disk antenna reported in [49] because of its wide bandwidth range. After some modifications, that antenna is transformed to 3-port version for different frequency ranges. It consists of a radiating disk and three microstrip lines for creating feeding mechanism. The dimensions of 3-port radiating element seen in Figure 5.3 are optimized to achieve 50 Ω matching at ports (S_{11}, S_{22}, and S_{33}) and good isolation from P_1 to P_2 and P_1 to P_3 (S_{12} and S_{13}).

The whole circuit can be divided into 3 parts – a radiating disk and microstrip feeding lines at the top layer and the etched ground plane at the bottom layer. The radius of planar disk and width and length of microstrip feeding lines are controlled by r, w_F, and h_F, respectively. The frequency range is calibrated by optimizing r and h_F, and 50 Ω matching

over this frequency range is determined by w_F. The radius of the planar disk (r) is initially selected as quarter-wavelength at 2.4 GHz which corresponds to 15.6 mm.

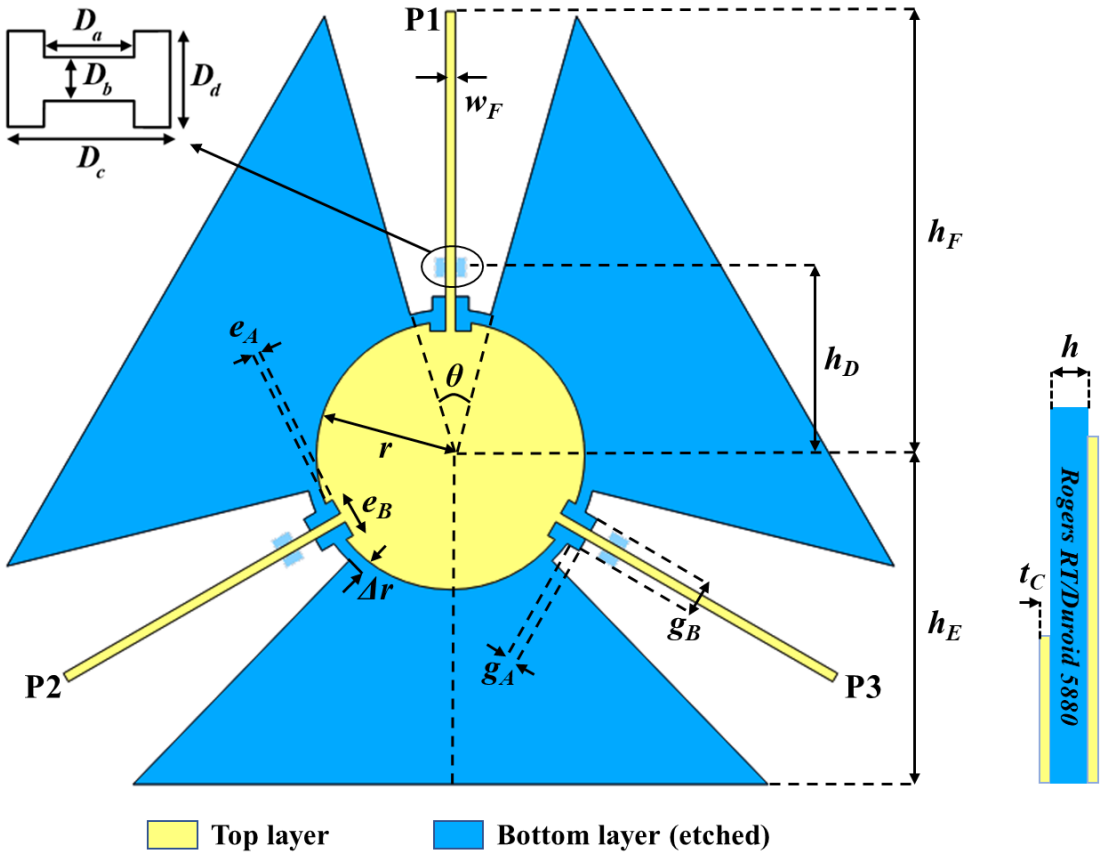

Figure 5.3: The 2D schematic of the designed 3-port radiating element

After parametric simulations, it is found that return loss bandwidth is enhanced although its starting frequency shifts to left, with the increment of r. Moreover, θ, h_E, and Δr check the shape of etching structure at the ground plane. The magnitude of isolation between P_1 to P_2 and P_1 to P_3 (S_{12} and S_{13}) is highly affected by θ, and h_F controls the magnitude of 50 Ω matching at P_1, P_2, and P_3. Additively, Δr affects 10 dB return loss frequency range of P_1, P_2, and P_3 (S_{11}, S_{22}, and S_{33}). The remaining dimensions are optimized to achieve better return loss and isolation bandwidth. Consequently, a 3-port radiating element with etched ground plane is designed using 0.79 mm thick Rogers RT/Duroid material (ε_r=2.2, tangent loss=0.0009). The optimized dimensions of parameters shown in Figure 5.3 are shown in Table 5.2.

Table 5.2: The dimensions of 3-port radiating element

Symbol	Dimension
r	22.1
w_F	1.6
h_F	73.2
θ	24
h_E	54.2
e_B	2.6
e_A	1.6
Δr	2
g_B	6
g_A	2.1
h_D	31
D_a	2
D_b	1.6
D_c	5
D_d	3.2
t_C	0.035
h	0.79

unit: mm

After the optimization of dimensions, the design is simulated with a high mesh number. Figure 5.4 shows simulated return loss (S_{11}, S_{22}, and S_{33}) and theoretically calculated interport isolation in case P_1 and P_2 are fed by signals with 180^0 of phase difference (S_{12} – S_{13}). Since the architecture is totally symmetrical, the reflection coefficient of P_1 (S_{11}) is equal to the reflection coefficient of P_2 and P_3 (S_{22}, S_{33}). According to the simulation results, the 3-port radiating element operates between 1.8 – 7.6 GHz with 5.8 GHz of 10 dB return loss bandwidth. For the proposed architecture, simulated isolation between P_1 and P_2 (S_{12}) is better than 13 dB over operation bandwidth, and similar case occurs between P_1 and P_3 (S_{13}), too. (S_{12} – S_{13}) operation can be performed by connecting a wideband balun between P_2 and P_3, thus, a very high interport isolation is achieved. As it is shown in Figure 5.4, the magnitude of (S_{12} – S_{13}) operation is higher than 53 dB over the antenna input bandwidth.

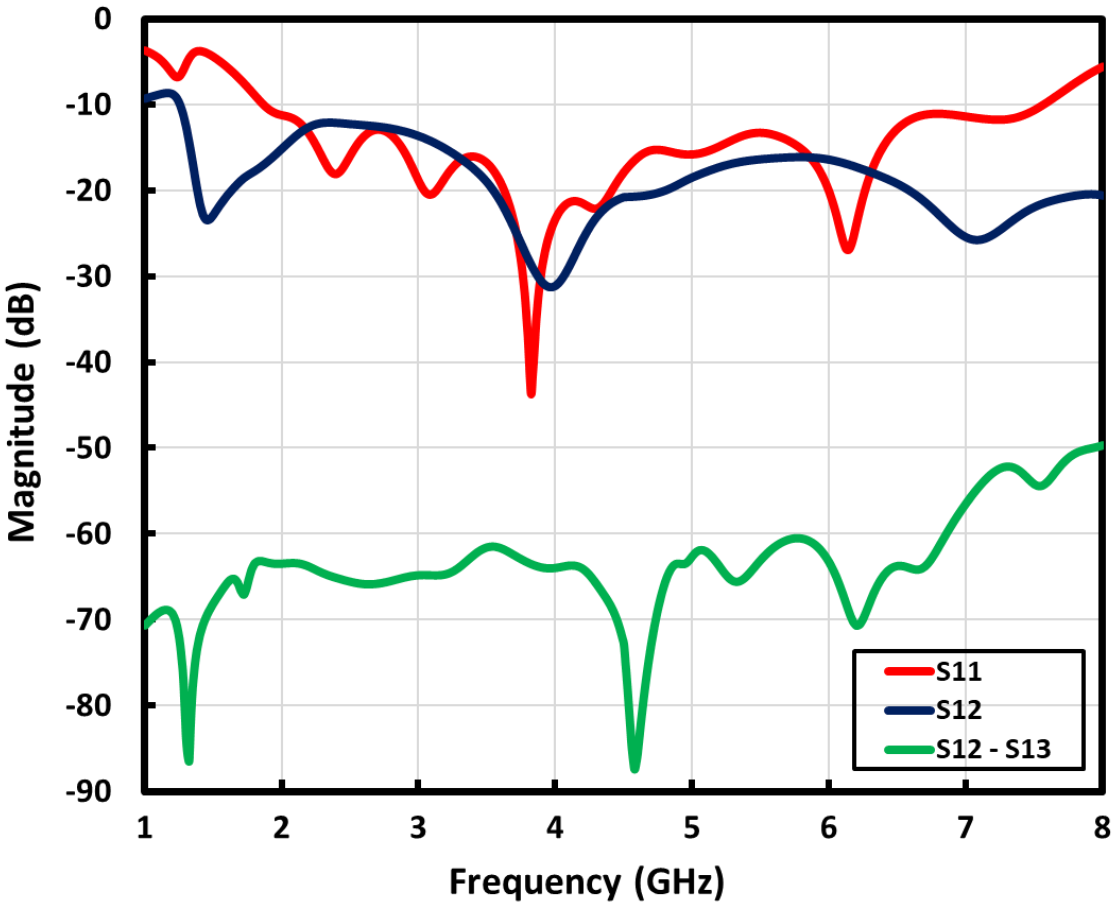

Figure 5.4: Simulated return loss (S_{11}) and isolation (S_{12}) with calculated ($S_{12} – S_{13}$) operation

5.2. Design Details and Simulation Analysis of UWB IBFD Antenna

The UWB IBFD antenna is designed uniting the three ports antenna with the UWB balun presented in previous parts. Since the objective is to start frequency band at 2.3 GHz, the radius of planar radiating disk (r) and the length of feed lines (hp) are determined as 23.1 and 73.2 mm, respectively. In case of arranging the operating frequency range at higher bands, the more compact antenna with half-size or quarter-size can be designed.

The top, bottom, and the cross-sectional view of the designed UWB IBFD antenna are shown in Figure 5.5. It has an area of 18 cm x 16 cm. While the top layer includes 3-port radiating element and microstrip lines of UWB balun, the bottom layer is created etching regions and slotline.

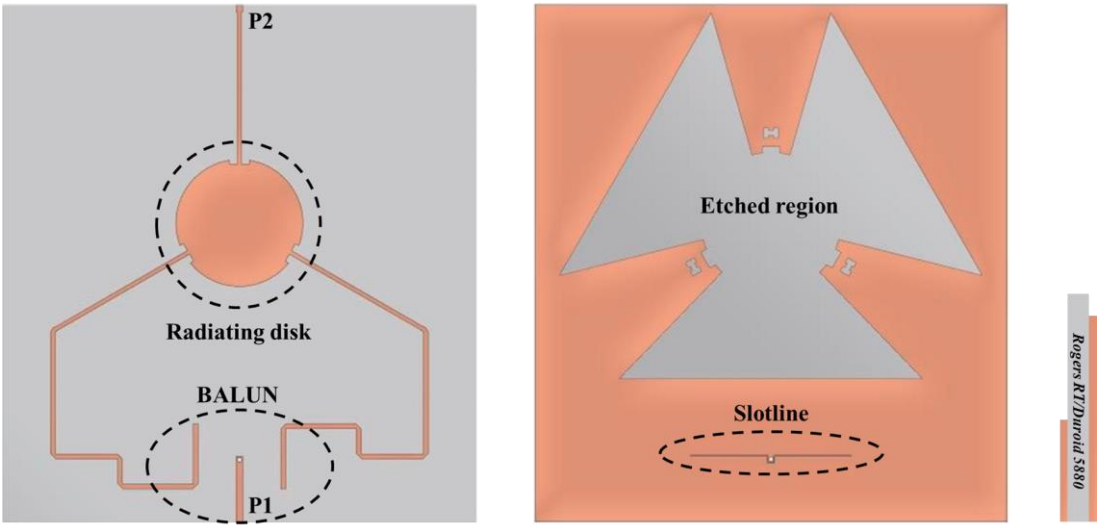

(a) (b) (c)

Figure 5.5: The designed UWB IBFD antenna (a) top view (b) bottom view (c) cross-sectional view

S-parameter simulation results of the designed UWB IBFD antenna are shown in Figure 5.6. The simulated results show the designed UWB IBFD antenna obtains higher than 35 dB of interport isolation over its input bandwidth of 5.1 GHz (2.1 – 7.3 GHz. Moreover, 40 dB of interport isolation is achieved between 3.5 – 5.9 GHz.

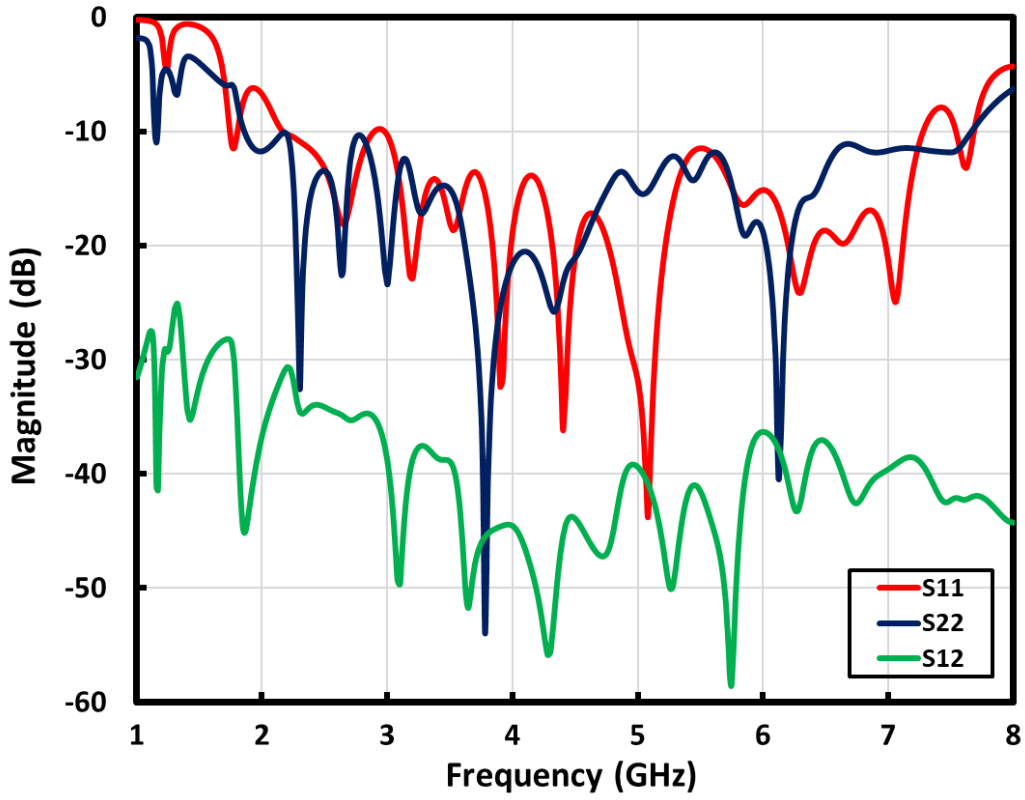

Figure 5.6: S-parameter simulation results of UWB IBFD antenna

Simulated peak realized gain results over the frequency of the designed UWB IBFD antenna is shown in Figure 5.7(a). As can be seen, peak realized gain over the frequency curves are different when the antenna is excited by P_1 and P_2. When the antenna is fed by P_1, it provides 4 – 8 dBi of peak realized gain for its 5.1 GHz of 10 dB return loss bandwidth. Furthermore, it reaches its maximum value at 6.2 GHz. The antenna provides 3 – 6 dBi of peak realized gain when it is fed by P_2.

Since there is an etched region at ground plane, the designed UWB IBFD antenna radiates to two different sides. Figure 5.7(b) shows the peak realized gain at 4.5 GHz over theta angle when the antenna is fed by P_2. According to the simulation results, the designed UWB IBFD antenna provides gain for $-73^0 < \theta < 15^0$ and $155^0 < \theta < 255$ for phi = 0^0, while the gain is positive for $-54^0 < \theta < 42^0$ and $116^0 < \theta < 210^0$ for phi = $90^{0.}$

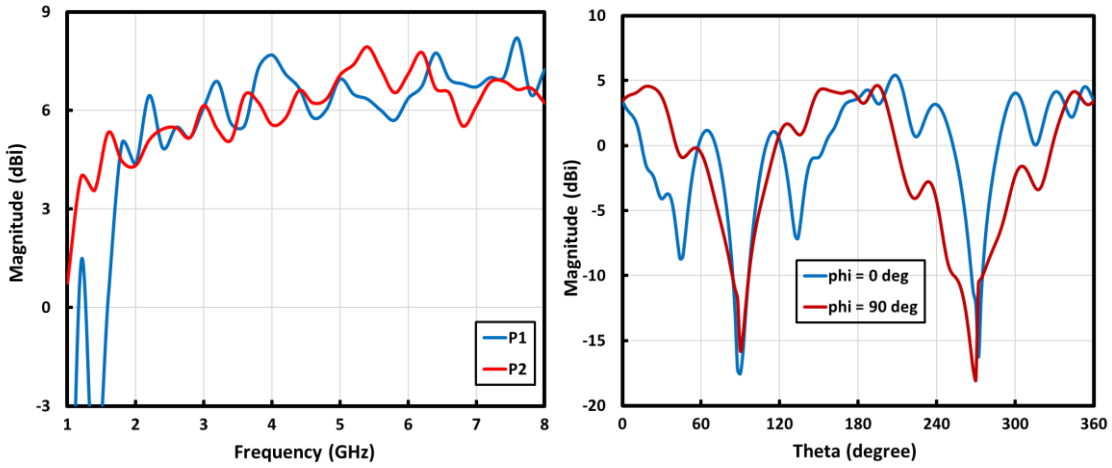

(a) (b)

Figure 5.7: Simulated realized gain patterns (a) versus frequency (b) versus theta angle for phi = 0 and phi = 90 at 4.5 GHz

5.3. Fabrication and Measurement Details of the UWB IBFD Antenna

UWB IBFD antenna has been fabricated using 0.79 mm thick Rogers RT/Duroid 5880 substrate (ε_r=2.2, tangent loss=0.0009). The top and bottom views of the implemented UWB IBFD antenna are shown in Figure 5.8(a) and 5.8(b), respectively.

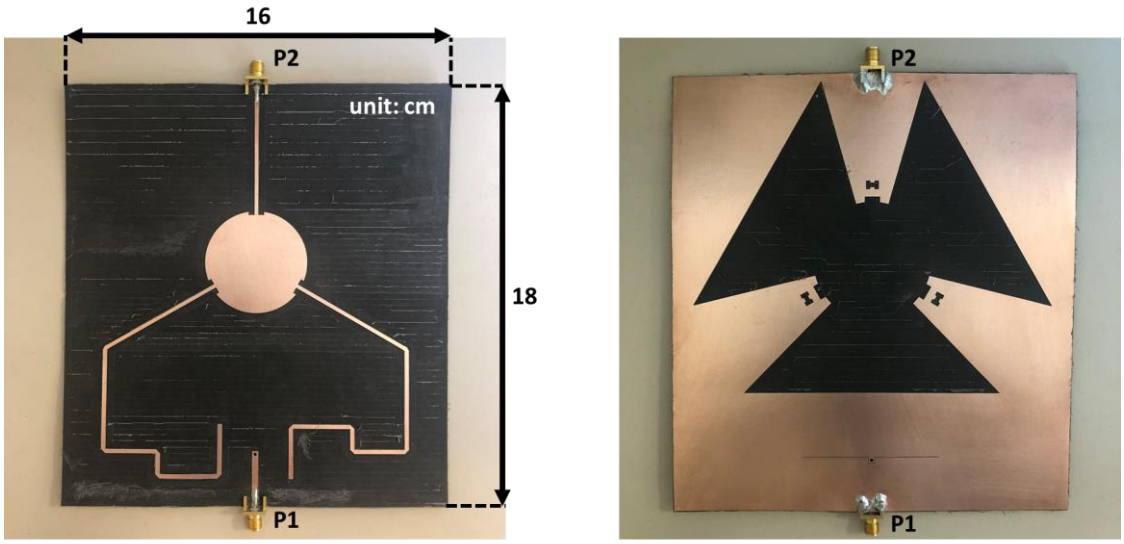

(a) (b)

Figure 5.8: (a) Top and (b) bottom views of the fabricated UWB IBFD antenna

S-parameter measurements have been performed by placing it among the RF absorbers to avoid RF reflections and environmental influences. SOLT (Short, Open, Load, Thru) calibration of Tx and Rx ports of Rohde & Schwarz FSH8 Network Analyzer [46] has been carried out with the help of Rohde & Schwarz ZV-Z135 Calibration Kit [47]. Figure 5.9 shows the different views of S-parameter measurement environment.

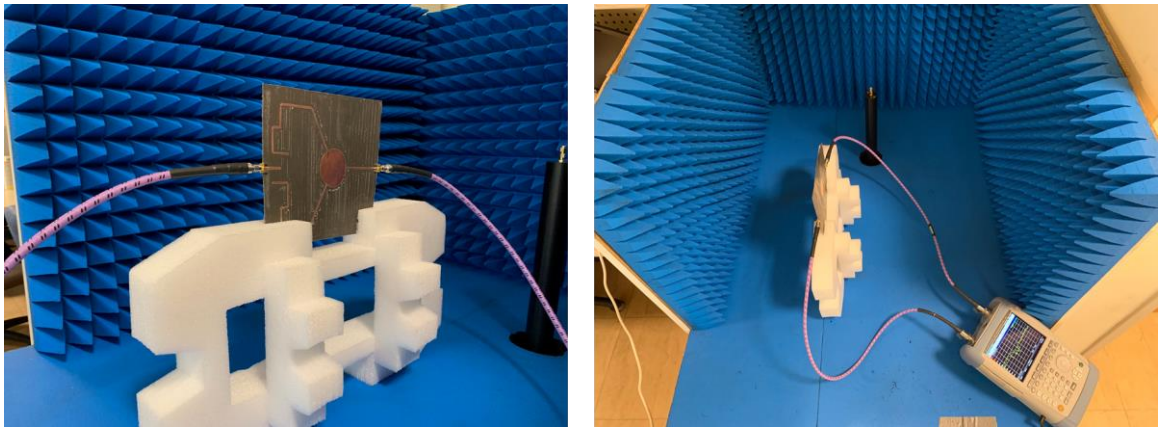

Figure 5.9: Different views of S-parameter measurement environment

The measured return loss (S_{11} and S_{22}) and isolation between P_1 and P_2 (S_{12}) results given in Figure 5.10 show that implemented UWB IBFD antenna achieves better than 30 dB of interport isolation over its 4.9 GHz of 10 dB return loss bandwidth (2.3 – 7.2 GHz). Moreover, better than 40 dB of interport isolation is provided over 1.2 GHz bandwidth (3.6 – 4.8 GHz). The maximum interport isolation of the antenna is approximately 63 dB at 3.75 GHz of frequency. It can be clearly said that S-parameter measurement results are very similar to simulation results.

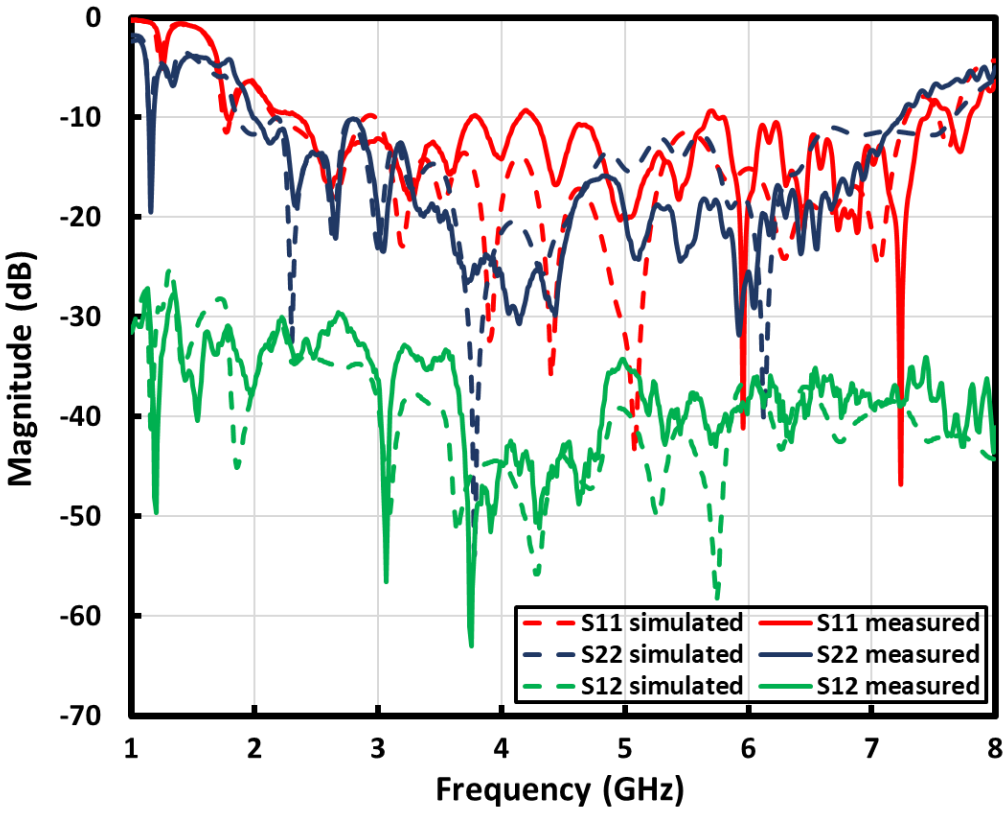

Figure 5.10: Measurement and simulation results of the UWB IBFD antenna

The gain measurements of the implemented UWB IBFD antenna have been performed at Sabancı University Nanotechnology Research and Application Center (SUNUM) [50]. To avoid all of RF reflections and any environmental impact, the antenna has been measured inside anechoic chamber. The measurement environment can be seen in Figure 5.11. The antenna gain depends on the port fed. Table 5.3 shows the peak realized gain values for different frequencies when the antenna is fed from P_1 and P_2.

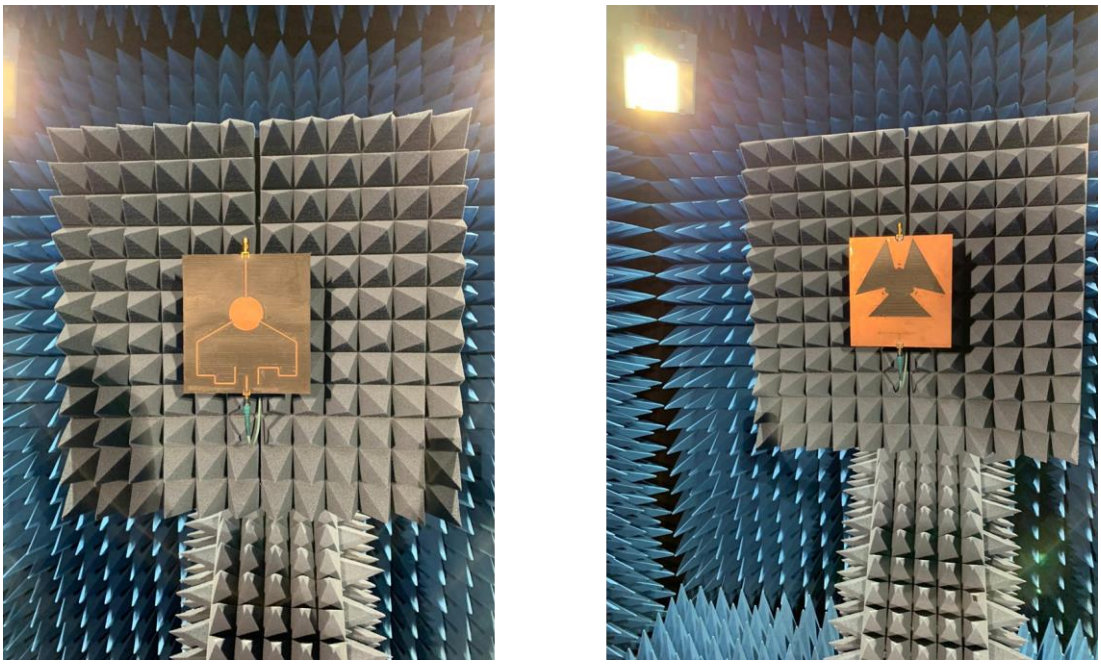

(a) (b)

Figure 5.11: The gain measurement environment of the UWB IBFD antenna (a) front-view (b) back-view

Table 5.3: Peak realized gain of the UWB IBFD antenna when it is fed from P_1 and P_2 for phi=0 and phi=90 degrees

Frequency/Port	**P1**	**P2**
2.4 GHz	4.35 dBi	3.66 dBi
3.6 GHz	5.58 dBi	4.96 dBi
5.8 GHz	6.74 dBi	2.92 dBi
6 GHz	7.83 dBi	5.14 dBi
6.6 GHz	8.26 dBi	4.51 dBi
7 GHz	7.47 dBi	6.44 dBi

The 2D polar plots of the simulated and measured realized gain at 2.4, 3.6, 5,8, 6, 6.6, and 7 GHz of frequencies can be seen in Figure 5.12. Due to 120^0 angle between differential fed microstrip feeding lines of the radiating disk, the polarization of the UWB IBFD antenna seems as elliptical. 180^0 of phase difference and 120^0 angle between microstrip feed lines cause elliptical polarization except linear polarization.

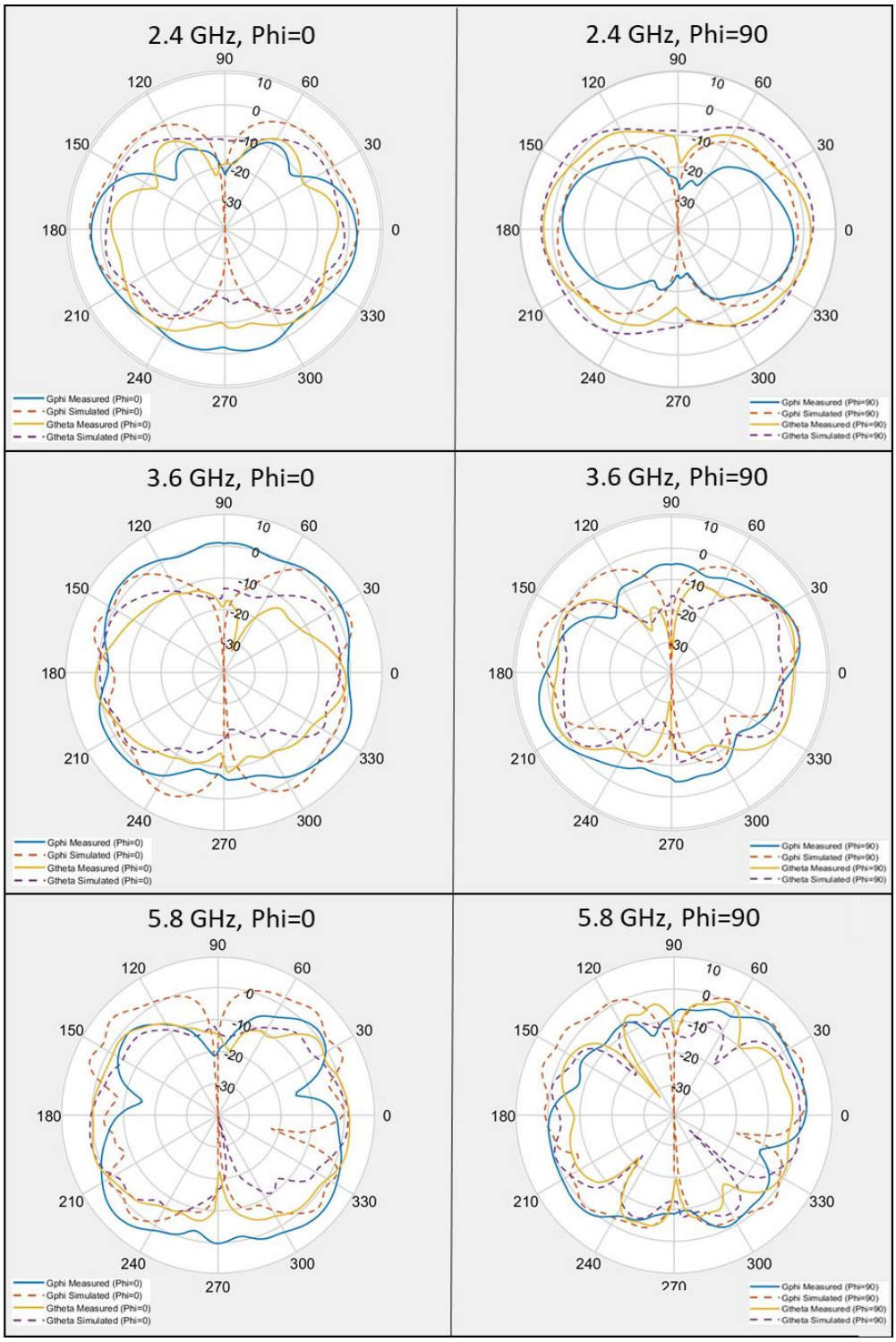

(a)

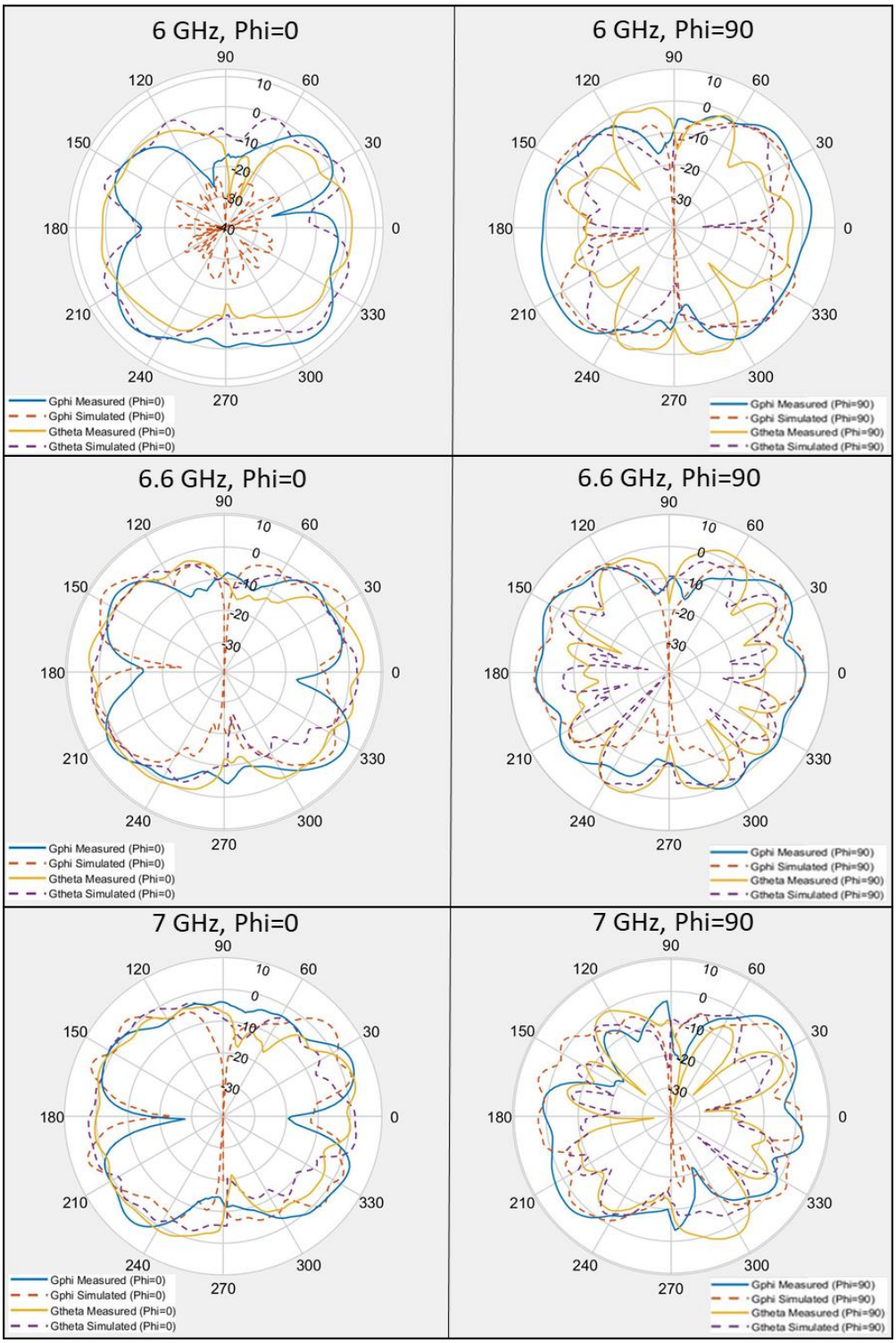

(b)

Figure 5.12: The 2D polar plots of simulated and measured gain of UWB IBFD antenna when it is fed from P_1 at (a) 2.4, 3.6 and 5.8 GHz (b) 6, 6.6 and 7 GHz

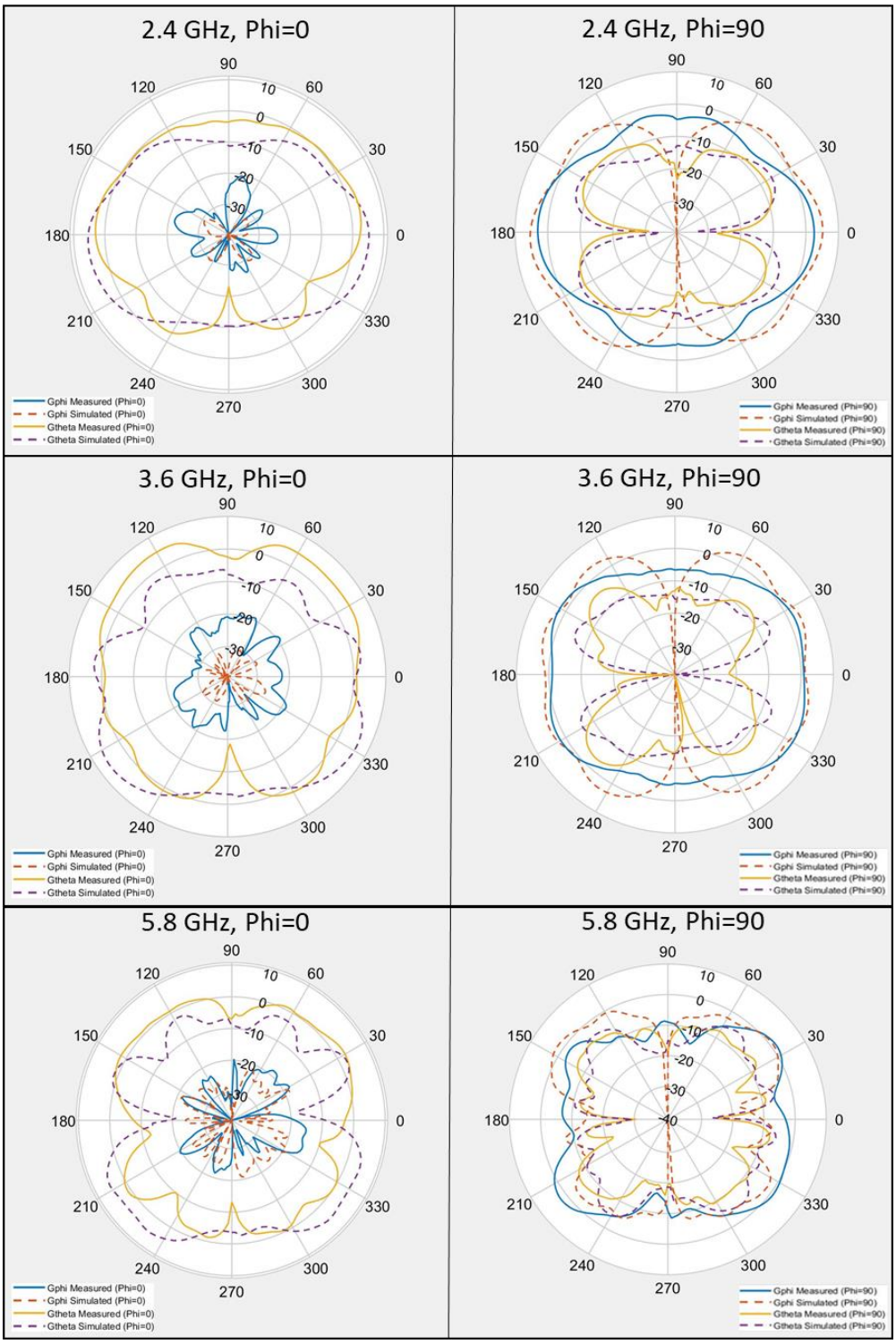
2.4 GHz, Phi=0
Gphi Measured (Phi=0)
Gphi Simulated (Phi=0)
Gtheta Measured (Phi=0)
Gtheta Simulated (Phi=0)
2.4 GHz, Phi=90
Gphi Measured (Phi=90)
Gphi Simulated (Phi=90)
Gtheta Measured (Phi=90)
Gtheta Simulated (Phi=90)
3.6 GHz, Phi=0
Gphi Measured (Phi=0)
Gphi Simulated (Phi=0)
Gtheta Measured (Phi=0)
Gtheta Simulated (Phi=0)
3.6 GHz, Phi=90
Gphi Measured (Phi=90)
Gphi Simulated (Phi=90)
Gtheta Measured (Phi=90)
Gtheta Simulated (Phi=90)
5.8 GHz, Phi=0
Gphi Measured (Phi=0)
Gphi Simulated (Phi=0)
Gtheta Measured (Phi=0)
Gtheta Simulated (Phi=0)
5.8 GHz, Phi=90
Gphi Measured (Phi=90)
Gphi Simulated (Phi=90)
Gtheta Measured (Phi=90)
Gtheta Simulated (Phi=90)

(a)

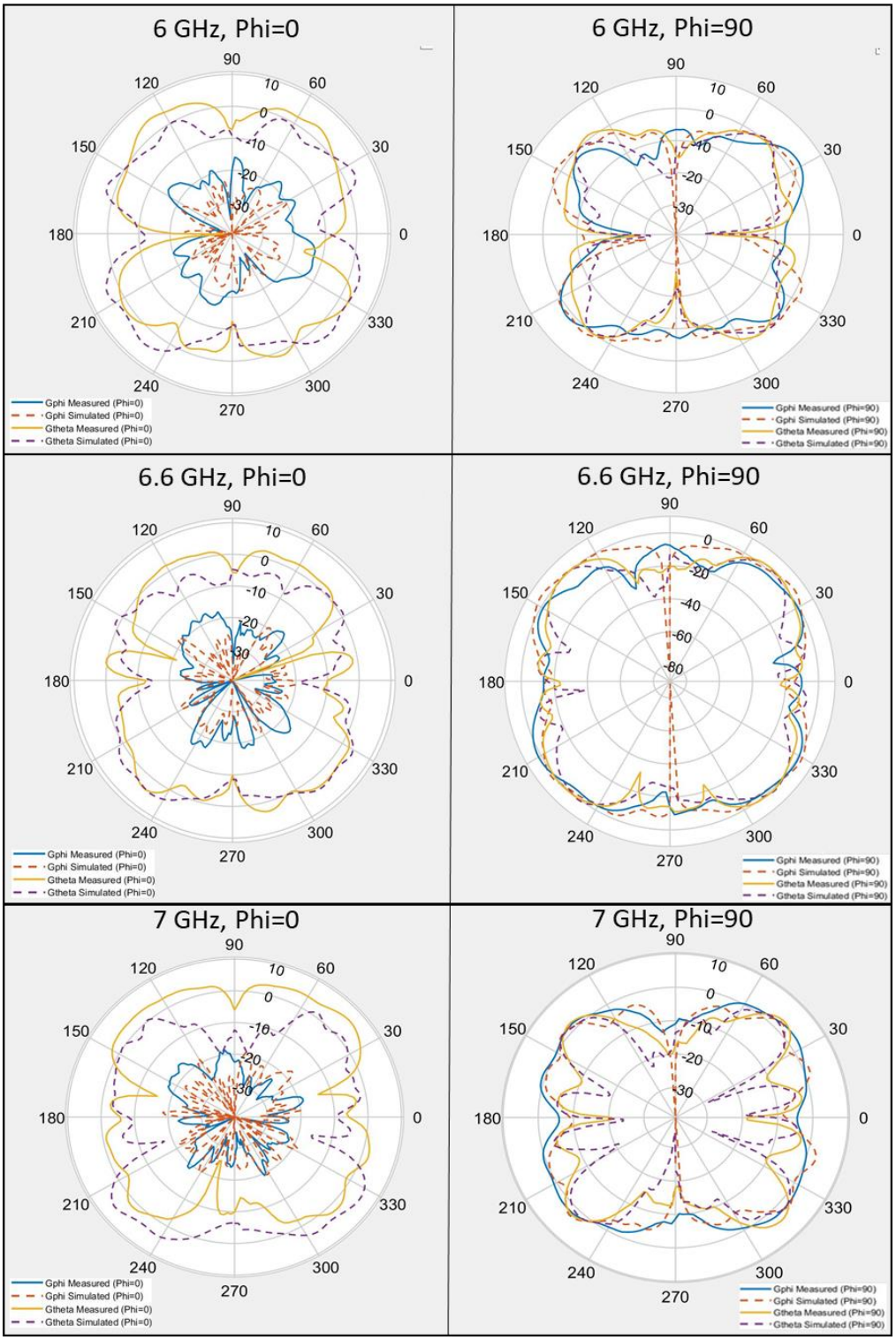

(b)

Figure 5.13: The 2D polar plots of simulated and measured gain of UWB IBFD antenna when it is fed from P_2 at (a) 2.4, 3.6 and 5.8 GHz (b) 6, 6.6 and 7 GHz

The peak realized gain values achieved by the UWB IBFD antenna when it is fed from P_1 and P_2 were given in Table 5.3. Figure 5.14 shows the comparison of simulation and measurement results of peak realized gain of the implemented UWB IBFD antenna. The antenna provides the gain of 8.26 dBi at 6.6 GHz when it is fed from P_1. On the other hand, it achieves the gain of 6.44 dBi at 7 GHz, when it is fed from P_2. According to the measurement results, the fabricated UWB IBFD antenna operates with high gain over its 10 dB return loss bandwidth.

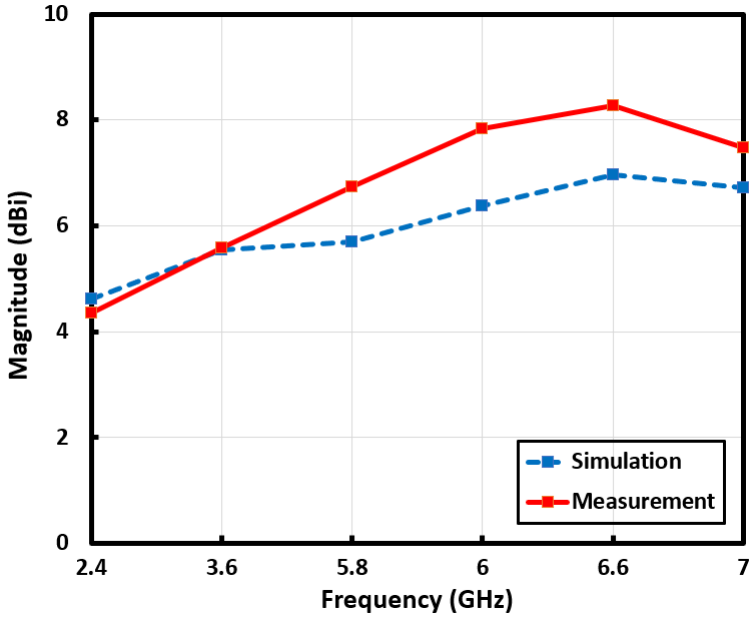

(a)

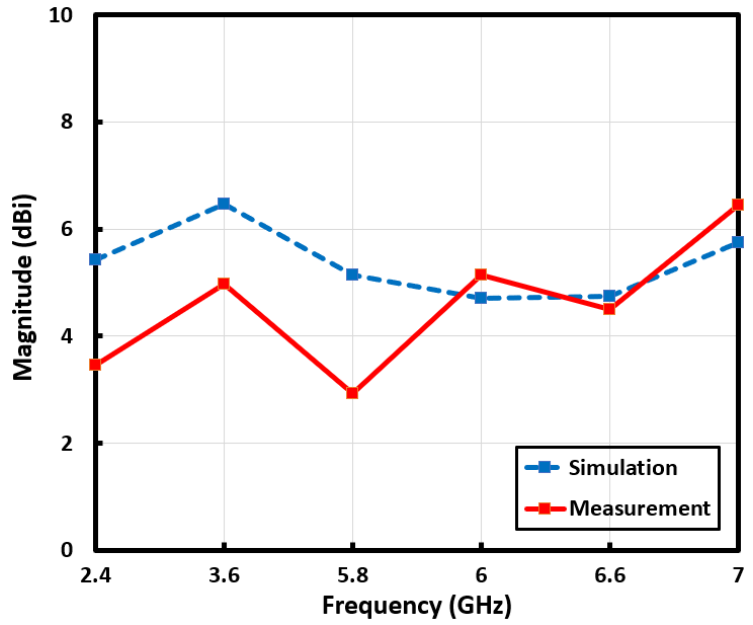

(b)

Figure 5.14: The simulation and measurement results of peak realized gain of the UWB IBFD antenna (a) when it is fed from P_1 (b) when it is fed from P_2

6. CONCLUSION AND FUTURE WORK

In this thesis, the design details, simulation analysis, and measurement details for three microstrip patch antennas and the UWB IBFD antenna are presented. Two of the proposed microstrip patch antennas operate at 2.4 GHz, while one of them operates at 5.8 GHz. Moreover, another antenna reported in this thesis called as UWB IBFD antenna operates from 2.3 to 7.2 GHz. The design, S-parameters simulations, radiation pattern simulations were performed using HFSS.

The architecture for all proposed antennas bases upon the same principal. The interport isolation is provided by shared antenna structure in addition to a SI cancellation circuit. Both antennas are differential fed in order to increase interport isolation. For feeding these antennas differential, microstrip balun is used as a differentiation circuit. Since its compact view, Marchand coupler is preferred as a microstrip balun circuit for 2.4 and 5.8 GHz antennas. The other microstrip balun circuits like ring hybrid coupler could be used instead of Marchand coupler. In addition, a compact UWB balun is designed and used for the implementation of the UWB IBFD antenna.

After introducing to IBFD communication systems and its literature review; design details, simulation results, and measurement performances of three microstrip patch antennas and UWB IBFD antenna are discussed. IBFD differential fed microstrip patch antenna array operated at 2.4 GHz obtains better than 53 dB of interport isolation for 50 MHz of 10 dB input bandwidth, in addition, higher than 65 dB of peak interport isolation is achieved. The same type antenna with different dimensions operated at 5.8 GHz achieves higher than 51 dB of isolation between its ports for 200 MHz of 10 dB return loss bandwidth. Its peak interport isolation is more than 78 dB. Frankly, it is more practical than 2.4 GHz version due to its size and operating bandwidth. Introduced IBFD

double differential fed microstrip patch antenna operated at 2.4 GHz consists of two different 1.6 mm thick FR4 substrates, the electrical connection between these substrates is provided with copper wires. This antenna ensures more than 62 dB for 50 MHz of 10 dB return loss bandwidth. Moreover, its peak isolation is more than 79 dB. The presented UWB IBFD antenna is fabricated on 0.79 mm thick Rogers RT/Duroid 5880 material whose dielectric constant is 2.2 and tangent loss is 0.0009. The implemented UWB IBFD antenna provides better than 30 dB of interport isolation for 4.9 GHz of operating bandwidth. To the best of our knowledge, there is no such an antenna that achieves this isolation value for such a wide bandwidth. Table 6.1 shows the comparison of the UWB IBFD antenna and the other introduced wideband antennas in literature.

Table 6.1: Interport isolation of UWB IBFD antenna compared to other reported wideband IBFD antennas in literature

	Antenna Input Bandwidth	**Interport Isolation for Antenna Input Bandwidth**
Lian et al. [19]	1.15 GHz	40 dB
Deo et al. [20]	2.2 GHz	21.5 dB
Wu et al. [21]	1.2 GHz	40 dB
Prasannakumar et al. [22]	4 GHz	30 dB
Amjadi et al. [23]	2.4 GHz*	54 dB
UWB IBFD Antenna	4.9 GHz	30 dB

*Input impedance bandwidth is calculated referencing 8 dB return loss.

It should be noted that measurements of three microstrip patch antennas were performed at the laboratory environment. Inside anechoic chamber, they could give better results. On the other side, S-parameter measurements of the UWB IBFD antenna are performed at semi-anechoic chamber in order to avoid RF reflections and any environmental effects. Furthermore, the gain measurements of the UWB IBFD antenna are carried out inside of anechoic chamber at Sabancı University Nanotechnology Research and Application Center (SUNUM).

If the proposed narrowband antennas are compared to each other, 2.4 GHz IBFD differential fed microstrip patch antenna array is the most compact product due to its size. However, 2.4 GHz IBFD double differential fed microstrip patch antenna provides the best interport isolation due to its design. Table 6.1 indicates interport isolation values provided for each proposed antenna in the thesis.

Table 6.2: Interport isolation values of proposed antennas

	Antenna Input Bandwidth	**Interport Isolation for Antenna Input Bandwidth**	**Peak Interport Isolation**
2.4 GHz IBFD Differential Fed Microstrip Patch Antenna Array	50 MHz	> 53 dB	> 65 dB
5.8 GHz IBFD Differential Fed Microstrip Patch Antenna Array	200 MHz	> 51 dB	> 78 dB
2.4 GHz IBFD Double Differential Fed Microstrip Patch Antenna	50 MHz	> 62 dB	> 79 dB
UWB IBFD Antenna	4.9 GHz	> 30 dB	> 62 dB

The proposed antennas offer a great solution to the SI problem which is the main challenge for the implementation of IBFD communication systems. These antennas can be used for many areas, like full duplex radar systems, full duplex relaying systems, and cognitive radios, as discussed earlier. The reported UWB IBFD antenna can be used for all of the Wi-Fi bands including 3.6 GHz and sub-6 GHz of 5G band.

IBFD double differential fed microstrip patch antenna was not designed for 3.6 GHz of operating frequency. Impedance bandwidth increases at higher frequencies; however, undesirable surface currents can decrease interport isolation. As a future work, the design and implementation of 3.6 GHz IBFD double differential fed microstrip antenna with high impedance bandwidth and interport isolation can be examined. Such an antenna can provide more interport isolation than proposed antennas. Another future work can be to design and implement the UWB IBFD antenna for higher frequencies for different applications and reaching a more compact size.

REFERENCES

[1] A. Sabharwal, P. Schniter, D. Guo, D. W. Bliss, S. Rangarajan and R. Wichman, "In-Band Full-Duplex Wireless: Challenges and Opportunities,", IEEE Journal on Selected Areas in Communications, vol. 32, no. 9, pp. 1637-1652, Sept. 2014. doi: 10.1109/JSAC.2014.2330193.

[2] P. S. Henry and Hui Luo, "WiFi: what's next?," in IEEE Communications Magazine, vol. 40, no. 12, pp. 66-72, Dec. 2002, doi: 10.1109/MCOM.2002.1106162.

[3] WiFi (Wireless Fidelity): http://www.wi-fi.org

[4] E. Khorov, I. Levitsky and I. F. Akyildiz, "Current Status and Directions of IEEE 802.11be, the Future Wi-Fi 7," in IEEE Access, vol. 8, pp. 88664-88688, 2020, doi: 10.1109/ACCESS.2020.2993448.

[5] B. Clerckx and C. Oestges, “MIMO-OFDMA System Level Evaluation,” in MIMO Wireless Networks: Channels, Techniques and Standards for Multi-Antenna, Multi-User and Multi-Cell Systems, 2nd ed. Oxford:Elsevier, 2013, pp. 663-665.

[6] H. Nawaz, “Dual Port Microstrip Patch Antennas and Circuits with High Interport Isolation for In-Band Full Duplex (IBFD) Wireless Applications”, Ph.D. Dissertation, Sabancı University, Jan. 2017.

[7] T. Riihonen, S. Werner and R. Wichman, "Mitigation of Loopback Self-Interference in Full-Duplex MIMO Relays," IEEE Transactions on Signal Processing, vol. 59, no. 12, pp. 5983-5993, Dec. 2011, doi: 10.1109/TSP.2011.2164910.

[8] E.A.E. Ahmed, “Self-interference Cancellation in Full-duplex Wireless Systems”, Ph.D. Dissertation, University of California, Irvine, 2014.

[9] M. E. Knox, "Single antenna full duplex communications using a common carrier," WAMICON 2012 IEEE Wireless & Microwave Technology Conference, pp. 1-6, Cocoa Beach, FL, 2012, doi: 10.1109/WAMICON.2012.6208455.

[10] W. T. Slingsby and J. P. McGeehan, "Antenna isolation measurements for on-frequency radio repeaters," 1995 Ninth International Conference on Antennas and Propagation, ICAP '95 (Conf. Publ. No. 407), vol.1, pp. 239-243, Eindhoven, Netherlands, 1995, doi: 10.1049/cp:19950300

[11] C. R. Anderson *et al.*, "Antenna Isolation, Wideband Multipath Propagation Measurements, and Interference Mitigation for On-frequency Repeaters," *IEEE* SoutheastCon, 2004. Proceedings, Greensboro, North Carolina, USA, 2004, pp. 110-114, doi: 10.1109/SECON.2004.1287906.

[12] K. Haneda, E. Kahra, S. Wyne, C. Icheln and P. Vainikainen, "Measurement of loop-back interference channels for outdoor-to-indoor full-duplex radio relays", Proceedings of the Fourth European Conference on Antennas and Propagation, Barcelona, 2010, pp. 1-5.

[13] E. Everett, A. Sahai and A. Sabharwal, "Passive Self-Interference Suppression for Full-Duplex Infrastructure Nodes", in IEEE Transactions on Wireless Communications, vol. 13, no. 2, pp. 680-694, February 2014. doi: 10.1109/TWC.2013.010214.130226

[14] L-Com. 2.4 GHz 90 degree dual-polarized antenna. https://www.l-com.com/multimedia/datasheets/DS_HG2414DP-090.PDF

[15] M. Jain, J. I. Choi, T. Kim, D. Bharadia, S. Seth, K. Srinivasan, P. Levis, S. Katti, and P. Sinha, “Practical, real-time, full duplex wireless,” Proc. 17th Annual International Conference on Mobile computing and Networking, 2011, pp. 301–312.

[16] N. Li, W. Zhu and H. Han, "Digital Interference Cancellation in Single Channel, Full Duplex Wireless Communication," 2012 8th International Conference on Wireless Communications, Networking and Mobile Computing, Shanghai, 2012, pp. 1-4, doi: 10.1109/WiCOM.2012.6478497.

[17] H. Nawaz and I. Tekin, "Dual-Polarized, Differential Fed Microstrip Patch Antennas With Very High Interport Isolation for Full-Duplex Communication," in IEEE Transactions on Antennas and Propagation, vol. 65, no. 12, pp. 7355-7360, Dec. 2017. doi: 10.1109/TAP.2017.2765829

[18] H. Nawaz and I. Tekin, "Double-Differential-Fed, Dual-Polarized Patch Antenna With 90 dB Interport RF Isolation for a 2.4 GHz In-Band Full-Duplex Transceiver," in IEEE Antennas and Wireless Propagation Letters, vol. 17, no. 2, pp. 287-290, Feb. 2018. doi: 10.1109/LAWP.2017.2786942

[19] R. Lian, T. Shih, Y. Yin and N. Behdad, "A High-Isolation, Ultra-Wideband Simultaneous Transmit and Receive Antenna With Monopole-Like Radiation

Characteristics," in IEEE Transactions on Antennas and Propagation, vol. 66, no. 2, pp. 1002-1007, Feb. 2018, doi: 10.1109/TAP.2017.2784447.

[20] P. Deo, D. Mirshekar-Syahkal, G. Zheng, A. Pal and A. Mehta, "BroadBand antenna for passive self-interference suppression in full-duplex communications," 2018 IEEE Radio and Wireless Symposium (RWS), Anaheim, CA, 2018, pp. 243-245, doi: 10.1109/RWS.2018.8304999.

[21] J. Wu, M. Li and N. Behdad, "A Wideband, Unidirectional Circularly Polarized Antenna for Full-Duplex Applications," in IEEE Transactions on Antennas and Propagation, vol. 66, no. 3, pp. 1559-1563, March 2018, doi: 10.1109/TAP.2018.2794063.

[22] P. Valale Prasannakumar, M. A. Elmansouri and D. S. Filipovic, "BroadBand Reflector Antenna With High Isolation Feed for Full-Duplex Applications," in IEEE Transactions on Antennas and Propagation, vol. 66, no. 5, pp. 2281-2290, May 2018, doi: 10.1109/TAP.2018.2814224.

[23] S. M. Amjadi and K. Sarabandi, "A Compact, BroadBand, Two-Port Slot Antenna System for Full-Duplex Applications," 2018 IEEE International Symposium on Antennas and Propagation & USNC/URSI National Radio Science Meeting, Boston, MA, 2018, pp. 389-390, doi: 10.1109/APUSNCURSINRSM.2018.8609125.

[24] M. Steer, Microwave and RF engineering: A systems approach. Scitech Publishing Inc., 2010.

[25] A. G. Stove, "Linear FMCW radar techniques," in IEE Proceedings F - Radar and Signal Processing, vol. 139, no. 5, pp. 343-350, Oct. 1992, doi: 10.1049/ip-f-2.1992.0048.

[26] R. A. Isberg and W. C. Y. Lee, "Performance tests of a low power cellular enhancer in a parking garage," IEEE 39th Vehicular Technology Conference, San Francisco, CA, USA, 1989, pp. 542-546 vol.2. doi: 10.1109/VETEC.1989.40128

[27] T. Riihonen, S. Werner and R. Wichman, "Mitigation of Loopback Self-Interference in Full-Duplex MIMO Relays," in IEEE Transactions on Signal Processing, vol. 59, no. 12, pp. 5983-5993, Dec. 2011. doi: 10.1109/TSP.2011.2164910

[28] H. Suzuki, K. Itoh, Y. Ebine and M. Sato, "A booster configuration with adaptive reduction of transmitter-receiver antenna coupling for pager systems," Gateway to 21st Century Communications Village. VTC 1999-Fall. IEEE VTS 50th Vehicular

Technology Conference (Cat. No.99CH36324), Amsterdam, The Netherlands, 1999, pp. 1516-1520 vol.3. doi: 10.1109/VETECF.1999.801547

[29] D. W. Bliss, P. A. Parker and A. R. Margetts, "Simultaneous Transmission and Reception for Improved Wireless Network Performance," 2007 IEEE/SP 14th Workshop on Statistical Signal Processing, Madison, WI, USA, 2007, pp. 478-482. doi: 10.1109/SSP.2007.4301304

[30] K.Ghosh, and A. Nath, "Cognitive Radio Networks: a comprehensive study on scope and applications," International Journal of Innovative Research in Advanced Engineering (IJIRAE), pp. 44-56, 2016.

[31] Y. Liang, K. Chen, G. Y. Li and P. Mahonen, "Cognitive radio networking and communications: an overview," in IEEE Transactions on Vehicular Technology, vol. 60, no. 7, pp. 3386-3407, Sept. 2011. doi: 10.1109/TVT.2011.2158673

[32] W. Cheng, X. Zhang, and H. Zhang, "Full duplex wireless communications for cognitive radio networks," arXiv:1105.0034v1, 2011.

[33] C. Deng et al., "IEEE 802.11be – Wi-Fi 7: New Challenges and Opportunities," in IEEE Communications Surveys & Tutorials, doi: 10.1109/COMST.2020.3012715.

[34] M. S. Elbamby, C. Perfecto, M. Bennis and K. Doppler, "Toward Low-Latency and Ultra-Reliable Virtual Reality," in *IEEE Network*, vol. 32, no. 2, pp. 78-84, March-April 2018, doi: 10.1109/MNET.2018.1700268.

[35] IEEE P802.11-TASK GROUP BE (EHT) MEETING UPDATE, http://www.ieee802.org/11/Reports/tgbe_update.htm

[36] L. Cariou, "802.11 EHT Proposed PAR," IEEE 802.11- 18/1231r6, Mar. 2019.

[37] D. Lopez-Perez, A. Garcia-Rodriguez, L. Galati-Giordano, M. Kasslin and K. Doppler, "IEEE 802.11be Extremely High Throughput: The Next Generation of Wi-Fi Technology Beyond 802.11ax," in IEEE Communications Magazine, vol. 57, no. 9, pp. 113-119, September 2019, doi: 10.1109/MCOM.001.1900338.

[38] L. Po-Kai et al., "Multi-Link Operation Framework," IEEE 802.11-19/0773r1, July 2019.

[39] ANSYS High Frequency Structure Simulator (HFSS), https://www.ansys.com/products/electronics/ansys-hfss

[40] D. Jorgesen and C. Marki, “Balun Basics Primer: A Tutorial on Baluns, Balun Transformers, Magic-Ts,and 180° Hybrids” https://www.aspen-electronics.com/uploads/3/7/1/2/37123419/balun_basics_primer-min.pdf , 2014 Marki Microwave, Inc.

[41] I. Lai, and M. Fujishima, “An Integrated Low-Power CMOS Up-Conversion Mixer Using New Stacked Marchand Baluns”, IEICE Transactions on Electronics E90C(4), doi: 10.1093/ietele/e90-c.4.823

[42] Keysight Advanced Design System (ADS), https://www.keysight.com/en/pc-1297113/advanced-design-system-ads

[43] Keysight E5062A Network Analyzer, http://literature.cdn.keysight.com/litweb/pdf/E5061-90140.pdf

[44] Keysight 85032E Calibration Kit, https://www.keysight.com/en/pd-1000000583%3Aepsg%3Apro-pn-85032E

[45] İTÜ RF Electronic Laboratory, http://www.rflab.itu.edu.tr/

[46] Rohde & Schwarz FSH8 Network Analyzer, https://www.rohde-schwarz.com/lt/product/zna-productstartpage_63493-551810.html

[47] Rohde & Schwarz ZV-Z135 Calibration Kit, https://scdn.rohde-schwarz.com/ur/pws/dl_downloads/dl_common_library/dl_brochures_and_datasheets/pdf_1/ZV-Z135_dat-sw_en_3606-6828-22_v0102.pdf

[48] S. Lin, J. Wang, Y. Deng and G. Zhang, "A new compact ultra-wideband balun for printed balanced antennas," Journal of Electromagnetic Waves and Applications, vol. 29, no. 12, pp. 1570-1579, May 2015, doi: 10.1080/09205071.2015.1051191.

[49] N. P. Agrawall, G. Kumar and K. P. Ray, "Wide-band planar monopole antennas," in IEEE Transactions on Antennas and Propagation, vol. 46, no. 2, pp. 294-295, Feb. 1998, doi: 10.1109/8.660976.

[50] Sabancı University Nanotechnology Research and Application Center (SUNUM), https://sunum.sabanciuniv.edu/